



Published in final edited form as:

Cell Rep. 2022 December 06; 41(10): 111742. doi:10.1016/j.celrep.2022.111742.

Crosstalk between pro-survival sphingolipid metabolism and complement signaling induces inflammasome-mediated tumor metastasis

Alhaji H. Janneh^{1,2}, Mohamed Faisal Kassir^{1,2}, F. Cansu Atilgan^{1,2}, Han Gyul Lee^{1,2}, Megan Sheridan^{1,2}, Natalia Oleinik^{1,2}, Zdzislaw Szulc^{1,2}, Christina Voelkel-Johnson^{1,2,3}, Hung Nguyen^{2,3}, Hong Li^{2,4}, Yuri K. Peterson^{2,5}, Elisabetta Marangoni⁶, Ozge Saatci⁷, Ozgur Sahin⁷, Michael Lilly², Carl Atkinson^{2,3}, Stephen Tomlinson^{2,3}, Shikhar Mehrotra^{2,3}, Besim Ogretmen^{1,2,8,*}

¹Department of Biochemistry and Molecular Biology, Medical University of South Carolina, 86 Jonathan Lucas Street, Charleston, SC 29425, USA

²Hollings Cancer Center, Medical University of South Carolina, 86 Jonathan Lucas Street, Charleston, SC 29425, USA

³Department of Microbiology and Immunology, Medical University of South Carolina, 86 Jonathan Lucas Street, Charleston, SC 29425, USA

⁴Department of Public Health, College of Medicine, Medical University of South Carolina, 86 Jonathan Lucas Street, Charleston, SC 29425, USA

⁵Department of Drug Discovery and Biomedical Sciences, College of Pharmacy, Medical University of South Carolina, 86 Jonathan Lucas Street, Charleston, SC 29425, USA

⁶Translational Research Department, Institut Curie, Paris, France

⁷Department of Drug Discovery and Biomedical Sciences, School of Pharmacy, University of South Carolina, Columbia, SC 29208, USA

⁸Lead contact

SUMMARY

Crosstalk between metabolic and signaling events that induce tumor metastasis remains elusive. Here, we determine how oncogenic sphingosine 1-phosphate (S1P) metabolism induces intracellular C3 complement activation to enhance migration/metastasis. We demonstrate that

This is an open access article under the CC BY-NC-ND license (<http://creativecommons.org/licenses/by-nc-nd/4.0/>).

*Correspondence: ogretmen@musc.edu.

AUTHOR CONTRIBUTIONS

Conception and design, A.H.J. and B.O.; methodology development, A.H.J., M.F.K., F.C.A., H.G.L., M.S., N.O., Z.S., C.V.-J., H.N., C.A., S.T., and B.O.; data acquisition, A.H.J., M.F.K., F.C.A., N.O., Y.K.P., E.M., O. Saatci, O. Sahin, and B.O.; data analysis and interpretation, A.H.J., H.L., Y.K.P., O. Saatci, O. Sahin, M.L., C.A., S.T., S.M., and B.O.; manuscript writing, review, and revision, A.H.J. and B.O.; administrative, technical, or material support, A.H.J. and B.O.; study supervision, B.O.

SUPPLEMENTAL INFORMATION

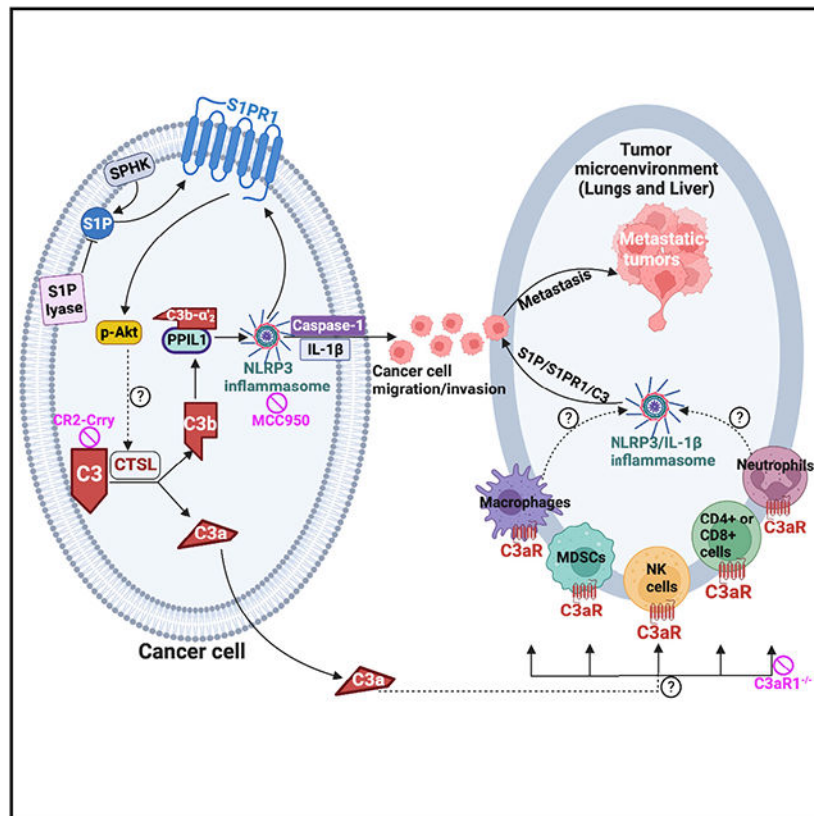
Supplemental information can be found online at <https://doi.org/10.1016/j.celrep.2022.111742>.

DECLARATION OF INTERESTS

The authors declare no competing interests.

increased S1P metabolism activates C3 complement processing through S1P receptor 1 (S1PR1). S1P/S1PR1-activated intracellular C3b- α_2 is associated with PPIL1 through glutamic acid 156 (E156) and aspartic acid 111 (D111) residues, resulting in NLRP3/inflammasome induction. Inactivation mutations of S1PR1 to prevent S1P signaling or mutations of C3b- α_2 to prevent its association with PPIL1 attenuate inflammasome activation and reduce lung colonization/metastasis in mice. Also, activation of the S1PR1/C3/PPIL1/NLRP3 axis is highly associated with human metastatic melanoma tissues and patient-derived xenografts. Moreover, targeting S1PR1/C3/PPIL1/NLRP3 signaling using molecular, genetic, and pharmacologic tools prevents lung colonization/metastasis of various murine cancer cell lines using WT and C3a-receptor1 knockout (C3aR1^{-/-}) mice. These data provide strategies for treating high-grade/metastatic tumors by targeting the S1PR1/C3/inflammasome axis.

Graphical Abstract



In brief

Janneh et al. define how sphingosine 1-phosphate (S1P) metabolism induces intracellular C3 complement activation to enhance cancer cell migration and metastasis via S1PR1/inflammasome signaling. Targeting the S1PR1/C3/inflammasome axis inhibits cancer cell migration/invasion and lung colonization, demonstrating the critical roles of the crosstalk between S1P metabolism and complement signaling in tumor metastasis.

INTRODUCTION

Cancer metastasis is the leading cause of solid-tumor-related deaths, and there is no reliable therapeutic intervention to prevent metastasis.^{1,2} Understanding the critical mechanisms involved in tumor metastasis will be clinically beneficial in targeting various solid tumors, including breast, prostate, bladder cancers, and melanoma, the most severe form of skin cancer that can spread to the lungs and brain. Recent studies demonstrated that sphingolipid metabolism, specifically sphingosine 1-phosphate (S1P), plays a crucial role in regulating cancer progression and metastasis.³⁻¹⁵

The sphingolipid metabolic pathway is a critical signaling process involved in diverse cellular functions, including cell proliferation, migration, invasion, and survival. S1P is a central lipid metabolite in the sphingolipid metabolic pathway, playing functional roles in the innate immune system, including the complement system that provides an initial defense mechanism against foreign pathogens. The functional roles of S1P are mediated through five known G-protein-coupled receptors, S1PR1-S1PR5.^{3,5,8,11,12} S1P generation is regulated by phosphorylation of sphingosine by sphingosine kinase 1 and 2 (SPHK1 and SPHK2). Intracellular S1P is rapidly catabolized with a half-life of about 8–10 min by S1P lyase.^{4,9} Sphingolipids, specifically ceramide and S1P, are biologically active molecules that regulate cellular processes such as survival, proliferation, migration, growth, and/or cell death.¹⁶ Ceramide is generally a potent inducer of cell death, which is hydrolyzed to yield sphingosine through the action of ceramidases, liberating sphingosine and fatty acids.^{17,18} Sphingosine is then phosphorylated by SPHK1 or SPHK2 to generate S1P, which signals through a family of G-protein-coupled receptors, GPCRs (S1P receptors 1–5, S1PR1-5) via a paracrine or autocrine manner to mediate cell growth, proliferation, and survival.¹⁹⁻²¹ Thus, a highly regulated metabolic balance exists between pro-apoptotic ceramide and pro-survival S1P to determine cancer cell fate for death or survival. Most cancer cells and tumors express increased SPHK1 and generate high levels of S1P, resulting in induction of growth, proliferation, drug resistance, and metastasis.²²⁻²⁴ S1P lyase catabolizes S1P, and inhibition of S1P lyase results in increased S1P accumulation, which then activates S1PR1. Interestingly, inhibition of S1PR2 also activates S1PR1.¹⁴ The specific mechanisms by which tumor cells induce S1P signaling to promote tumor metastasis are largely unknown.

The complement system is part of the innate immune system that can play a role in eliminating pathogens.^{25,26} Traditionally it was believed that the complement system had an anti-tumorigenic role by targeting and killing cancer cells.²⁷ However, in a shift from this paradigm, it was demonstrated that certain tumors could activate complement and that complement activation products can promote tumor cell survival and metastasis.^{28,29} The complement activation products that have roles in this process are C3a and C5a, which can be generated in the tumor microenvironment (TME) and signal through their respective receptors C3aR, C5aR1, or C5aR2. Furthermore, S1P levels in plasma and tissues are thought to be maintained by SPHK1-generated S1P in host immune blood and endothelial cells.³⁰ In addition, recent studies have demonstrated that the C5a activation product, via its interaction with C5aR1 on various cell types, stimulates intracellular SPHK1 activation and S1P release.³¹⁻³⁴ However, how complement signaling promotes cancer cell migration and

tumor metastasis and how complement activation is regulated by sphingolipid metabolism in the TME remains largely unknown.

In this study, we determine how intracellular complement signaling is regulated by S1P metabolism in cancer cells to facilitate the crosstalk between cancer and TME for inflammasome activation, leading to enhanced cancer cell migration/invasion and tumor metastasis. Our data also show that targeting the S1P/complement/inflammasome signaling axis inhibits tumor metastasis *in vivo*, providing mechanism-based strategies for treating high-grade/metastatic solid tumors, including melanoma and triple-negative breast cancer.

RESULTS

Induction of intracellular S1P signaling enhances cancer cell migration via complement C3 activation

In addition to the systemic roles of S1P, usually via paracrine signaling through S1PR1-5, intracellular S1P signaling plays a vital role in inducing cancer cell growth, progression, and migration through autocrine S1PR1 signaling. However, downstream mechanisms whereby intracellular S1P signaling induces migration/invasion/metastasis via crosstalk with intracellular complement signaling and whether autocrine (endogenous) S1PR1 signaling is involved in this process are mostly unknown. To delineate the roles of endogenous S1P/S1PR1 in the regulation of cancer cell growth and migration, we forced intracellular S1P accumulation and S1PR1 signaling by inhibiting S1P lyase using DPO,³⁵ which prevents the catabolism of endogenous S1P in the absence/presence of JTE-013, an antagonist of S1PR2 that induces S1PR1 expression/signaling.¹⁴ Induction of intracellular signaling of S1P/S1PR1 using DPO and JTE-013 in combination increased the migration of B16 murine melanoma cells ~5-fold compared with vehicle-treated controls and 2.5-fold compared with single-agent-treated cells (Figure 1A, left panel), without affecting cell growth/proliferation (Figure 1A, top right panel). Induction of intracellular S1P accumulation and signaling in response to JTE-013/DPO also increased complement protein C3 expression and processing (cleavage) ~3-fold compared with vehicle-treated controls, detected by western blotting using an anti-C3 antibody that detects C3b- α and C3b- β chains³⁶ (upper bands, Figure 1B), including the cleaved/activated C3b- α '₁ and C3b- α '₂ (iC3b) products (lower bands, Figure 1B). Consistently, JTE-013/DPO treatment of B16 cells increased intracellular C3a expression (Figure 1C, left panel) and secretion into the growth medium (Figure 1C, right panel) compared with vehicle-treated control. Effects of JTE-013/DPO on intracellular S1P and dihydro (dh)-S1P accumulation compared with controls were confirmed by lipidomics, consistent with decreased sphingosine (Sph) and dh-Sph (Figure 1D). Similarly, in other solid tumors, such as 4T1 breast, Myc-CaP prostate, and MB49 bladder cancer cells, induction of S1P signaling by JTE-013/DPO increased migration and C3 cleavage/activation (Figures S1A-S1C).

To determine if C3 plays any role in S1P-mediated cell migration, we knocked down the expression of C3 using shRNA and measured its effects on C3 abundance and B16 cell migration. shRNA-mediated knockdown of C3 reduced C3 expression by 80%, without significantly affecting S1PR1 protein expression levels (Figures 1E and 1F), and almost completely blunted S1P-mediated B16 cell migration (Figures 1G and 1H) in response

to JTE-013/DPO compared with Scr-shRNA-transfected controls. In reciprocal studies, ectopic expression of C3b- α' ₂ (Figure 1I) enhanced B16 cell migration ~2-fold in the absence/presence of JTE-013/DPO compared with vector-transfected controls (Figure 1J). On the other hand, inhibition of S1PR1 signaling using Ex26³⁹ abrogated C3b- α' ₂-mediated migration of B16 cells compared with controls (Figure 1J). Moreover, in addition to pharmacologic inhibition of S1P lyase, its shRNA-mediated knockdown (Figure 1K) with/without JTE-013 also induced B16 cell migration (Figure 1L) and increased C3 expression (Figures 1M and 1N) compared with Scr-shRNA-transfected cells. To determine the effects of exogenous S1P and JTE-013 on cell migration and invasion, we treated cells with either high-density lipoprotein (HDL)-bound S1P or albumin (BSA)-bound S1P, which are known carriers of S1P in a physiological context. Compared with BSA-bound S1P, HDL-bound S1P further increased B16 cell migration (Figure 1O) and invasion (Figure 1P). These data suggest that intracellular S1P accumulation in response to S1P lyase knockdown or inhibition, and treatment of cells with exogenous S1P with S1PR1 activation by S1PR2 inhibition using JTE-013, induce cancer cell migration and invasion via a mechanism involving C3 activation product C3b- α' ₂. Also, these results reveal that targeting C3 and S1PR1 signaling inhibits cancer cell migration and invasion.

Endogenous S1P induces cancer cell migration via S1PR1 signaling

To establish the roles of intracellular S1P signaling in inducing cancer cell migration possibly via autocrine S1PR1 signaling, we measured the effects of ectopic expression of S1PR1 (Figures 2A and 2B) on C3 expression and activation and B16 cell migration. Ectopic expression of S1PR1 increased B16 cell migration ~2-fold (Figure 2C), consistent with elevated S1P levels (Figure 2D), compared with vector-transfected controls, similar to the effects seen in JTE-013/DPO-treated cells. The induction of endogenous S1P signaling by S1PR1 overexpression was also determined by the activation of AKT, a known downstream target of S1P/S1PR1 signaling (Figure 2E, upper panel). Forced S1PR1 signaling also elevated C3 expression and activation compared with vector-only-transfected cells (Figure 2E, lower panel). Studies have shown that, unlike albumin-bound S1P, which tends to degrade S1PR1 over time, S1PR1 signaling relies more on HDL-bound S1P for its downstream activation of AKT.^{10,40} Therefore, we sought to determine the cell migration effects of BSA-bound S1P and HDL-bound S1P on S1PR1 overexpression cells. Treatment of B16 cells stably expressing S1PR1 with HDL-bound S1P, but not BSA-bound S1P, further increased B16 cell migration compared with vehicle-treated controls (Figure 2F). Moreover, inhibition of S1PR1 using a small-molecule antagonist, Ex26,³⁹ largely prevented HDL-S1P-mediated migration compared with controls (Figure 2F), supporting a role for the S1P/S1PR1/complement axis in inducing B16 cell migration. Moreover, inhibiting AKT with a highly selective inhibitor, MK-2206 2HCL, attenuated S1PR1-mediated cell migration (Figure 2G) and decreased C3 expression compared with untreated controls (Figures 2H and 2I), demonstrating the role of AKT in the S1P/S1PR1/C3 axis in inducing cell migration. Consistently, treating cells that stably overexpress S1PR1 with Ex26 decreased C3 expression compared with untreated controls (Figures 2H and 2I). These data reveal that endogenous S1P/S1PR1 signaling induces cell migration/invasion through AKT-mediated complement C3 activation in various cancer cells.

The C3-PPIL1 complex transduces intracellular S1P/S1PR1-mediated complement signaling

To determine how endogenous complement activation by intracellular S1P/S1PR1 signaling induces cancer cell migration, we identified C3-associated proteins in response to JTE-013/DPO exposure in B16 cells compared with vehicle-treated cells by co-immunoprecipitation (co-IP) using anti-C3 antibody followed by proteomics. In addition, we used an anti-IgG antibody as a negative control in co-IP studies. We identified six proteins whose association with C3 was enhanced in response to JTE-013/DPO (Figure 2J, left panel), and we could only validate the increased association of C3 with peptidyl-prolyl isomerase like 1 (PPIL1)^{41,42} by co-IP (Figure 2J, right panel) and PLA (Figures 2K and 2L), which showed ~2- to 4-fold enhanced C3-PPIL1 interaction. Also, CRISPR-Cas9-mediated silencing of PPIL1, which did not significantly affect S1PR1 protein expression levels (Figure 2M), prevented B16 cell migration in response to JTE-013/DPO-mediated S1P signaling (Figure 2N), suggesting a pivotal role for PPIL1 in the regulation of B16 migration by S1P/S1PR1/C3 signaling. Moreover, RNA-seq data showed that, while S1P/S1PR1 activation by JTE/DPO-induced expression of various complement (Figure 2O) and cell migration-associated (Figure 2P) genes, including C1qbp, C2, and C1rl, or VEGF, Pdgfr, H-ras, and Prkcq, respectively, knockdown of PPIL1 largely blunted the expression of these complement and cell migration-associated genes compared with controls, vector-only-transfected and vehicle-treated cells (Figures 2O and 2P, respectively). In addition, RNA-seq data showed that JTE/DPO-mediated S1P/S1PR1 activation induced the expression of genes known to be involved in inflammasome activation, including Pycard, Nfkb1, Sirt2, and Nlr4, compared with controls (Figure 2Q). CRISPR-Cas9-mediated silencing of PPIL1 also prevented the expression of these inflammasome-associated genes in response to JTE/DPO exposure (Figure 2Q), suggesting that activation of S1P/S1PR1 signaling induces cell migration and inflammasome activation via complement/PPIL1 complex.

To further understand the clinical relevance of S1PR1/C3 signaling in metastasis, we sought to utilize cell lines that do not require the forced expression of these proteins or pharmacologic induction of endogenous S1P. Consistently, in MDA-MB-231 human progression series cell lines, LM2-4175 (isolated from mice lung metastasis) and BOM-1833 (isolated from mice bone metastasis),⁴³ increased migration was highly associated with increased expression of endogenous S1PR1 and C3b- α' ₂ or induced C3-PPIL1 complex (Figures S1D, S1E, S1F-S1G, or S1H-S1J), respectively. Furthermore, to explore the specific roles of endogenous S1PR1/C3 signaling in cancer cell migration and invasion without any forced protein expression or induction of endogenous S1P with pharmacological inhibitors, we utilized metastatic UM-SCC-2B human head and neck squamous cell carcinoma cells, which exhibited increased cell migration and invasion compared with parental non-metastatic UM-SCC-22A cells (Figures S2A-S2E). UM-SCC-22B cells had decreased expression of S1P lyase, SGPL1 (Figure S2F and S2G), consistent with increased SPHK1 expression (Figures S2F and S2G) and S1P accumulation (Figure S2G) or S1PR1 levels (Figures S2H-S2K) compared with UM-SCC-22A cells. Increased S1PR1 and C3 expression were also consistent with inflammasome activation, detected by overexpressed NLRP3, active-caspase-1, or cleaved-IL-1 β in UM-SCC-22B compared with UM-SCC-22A cells (Figures S2L and S2M). C3 activation was also

confirmed by increased levels of endogenous C3a (Figures S2L and S2M) and secreted C3a into the growth medium (Figure S2N). Notably, the association between C3 and PPIL1 was also increased in metastatic UM-SCC-22B compared with controls (Figures 3A-3C). Pharmacologic inhibition of S1PR1 or inflammasome signaling using Ex26 or MCC950, respectively, prevented the migration of UM-SCC-22B cells compared with their vehicle-treated controls (Figures 3D and 3E), which was consistent with decreased expression of S1PR1 or NLRP3 and C3, cleaved-IL-1 β or active-caspase-1 in response to Ex26 or MCC950 in UM-SCC-22B cells (Figure 3F).

Next, we measured the effects of shRNA-mediated knockdown of C3 or CRISPR-Cas9-mediated silencing of S1PR1 or NLRP3 on C3-PPIL1 association, inflammasome activation, and cell migration in UM-SCC-22B cells. Knockdown of C3 (Figures 3G, upper panel, and 3H) resulted in the reduction of NLRP3, cleaved-IL-1 β , or active-caspase-1 expression compared with Scr-shRNA-transfected cells (Figure 3G, middle and lower panels). Also, CRISPR-Cas9 silencing of S1PR1 or NLRP3 (Figures 3I-3K) decreased cleaved-IL-1 β or active-caspase-1 expression (Figure 3I, middle and lower panels) compared with vector-transfected UM-SCC-22B cells. Interestingly, CRISPR-Cas9 silencing of NLRP3 also decreased S1PR1 at the protein level and, to a lesser extent, at the mRNA levels (Figures 3I and 3J), indicating a possible positive feedback loop mechanism between NLRP3 and S1PR1 signaling in metastatic cancer cells.

The association between C3 and PPIL1 plays a critical role in S1P/S1PR1-mediated inflammasome activation and cell migration

To determine whether C3 and S1PR1 signaling plays a role in inflammasome activation and migration via the C3-PPIL1 complex, we measured the effects of shRNA-dependent knockdown of C3 on C3-PPIL1 interaction or cell migration in UM-SCC-22B cells compared with Scr-shRNA-transfected controls. Data demonstrated that C3 knockdown almost completely blunted the C3-PPIL1 association, which appears to be higher in the cytoplasm than in the nuclei (Figures 3L and 3M) and decreased cell migration (Figures 3N and 3O) in UM-SCC-22B cells compared with controls. Similarly, CRISPR-Cas9-mediated S1PR1 silencing reduced C3-PPIL1 interaction (Figures 3P and 3Q), consistent with reduced cell migration (Figures S3A and S3B). S1PR1 silencing also decreased intracellular C3a expression (Figures S3C and S3D) and reduced the levels of secreted C3a (Figure S3E) in UM-SCC-22B compared with their vector-only-transfected controls. Moreover, CRISPR-Cas9-dependent NLRP3 silencing also inhibited cell migration in UM-SCC-22B compared with their vector-only-transfected controls (Figures S3A and S3B). In UM-SCC-22B cells, knockdown of C3 and silencing of S1PR1 or NLRP3 also prevented mRNA expression of some inflammasome-related genes, including NLRP3 (used to confirm knockdown) and IL-1 β compared with their controls (Figures S3F-S3I).

To determine the role of S1P/S1PR1 signaling in C3-PPIL1 association and inflammasome activation, we expressed vector-only, or WT-S1PR1 versus mutant S1PR1 with R120A or W269L (Figures 4A-4C) conversions that are known to inhibit S1PR1 activation by S1P, in B16 melanoma cells. As a result, ectopic expression of WT-S1PR1, but not R120A-S1PR1 or W269L-S1PR1, increased C3 expression and enhanced cell migration

compared with vector-only-transfected controls (Figures 4D and 4E). Also, while WT-S1PR1 expression increased the association between C3 and PPIL1, R120A-S1PR1 or W269L-S1PR1 failed to induce the C3-PPIL1 complex compared with controls (Figures 4F and 4G). Moreover, CRISPR-Cas9-mediated silencing of PPIL1, without significantly affecting S1PR1 expression (Figure 4H), blunted the migration of B16 cells expressing WT-S1PR1 compared with controls (Figure 4I). These data were also consistent with the effects of PPIL1 silencing on preventing WT-S1PR1-mediated activation of the inflammasome, detected by NLRP3, caspase-1 (precursor and active), and IL-1 β (precursor and cleaved) expression levels compared with controls (Figure 4J). Similarly, PPIL1 silencing also prevented JTE-013/DPO-induced NLRP3 inflammasome as detected by NLRP3 protein expression compared with controls (Figure 4K). These data support that S1P/S1PR1 signaling induces cell migration via NLRP3-mediated inflammasome activation through the C3-PPIL1 complex.

To interrogate the roles of the C3-PPIL1 complex in inducing cell migration through inflammasome activation, we began by performing biomolecular docking simulations. Our molecular modeling was based on X-ray structural information (Figures 5A and 5B) and identified several residues that might play vital roles in C3b- α' ₂-PPIL1 association and interaction, including D111 and E156. Based on this information, we generated three C3b- α' ₂ mutants as follows; C3b- α' ₂^{D111A}, C3b- α' ₂^{E156A}, and C3b- α' ₂^{D111A, E156A} (2X, double mutant). All three mutants were stably expressed in B16 melanoma cells (Figures 5C-5E). The data showed that, while ectopically expressed WT-C3b- α' ₂-associated with PPIL1, all three mutations altered C3b- α' ₂ association with PPIL1 (Figures 5F and 5G). These data were also consistent with the induction of migration and inflammasome activation by WT-C3b- α' ₂, but not its mutant that does not associate with PPIL1 due to C3b- α' ₂^{D111A}, C3b- α' ₂^{E156A}, and C3b- α' ₂^{D111A, E156A} conversions, compared with vector-only-transfected B16 control cells (Figures 5H and 5I). Interestingly, CRISPR-Cas9-dependent silencing of PPIL1, without significantly affecting the expression of S1PR1 (Figure 5J), attenuated WT-C3b- α' ₂-mediated B16 cell migration and inhibited NLRP3/inflammasome activation (Figures 5K and 5L). Similarly, inhibition of NLRP3 inflammasome using MCC950 almost completely prevented cell migration in response to WT-C3b- α' ₂ overexpression (and to a lesser extent in response to S1PR1 overexpression) compared with vehicle-treated controls (Figure 5M). These data were consistent with the inhibition of IL-1 β and caspase-1 activation by MCC950 in response to C3b- α' ₂ or S1PR1 overexpression (Figure 5N). In addition, inhibiting AKT with MK-2206 2HCl and NLRP3/inflammasome activation with MCC950 in response to C3b- α' ₂ overexpression did not have any significant effect on S1PR1 expression at protein (Figure 5O) or mRNA levels (Figure 5P) compared with untreated controls. Thus, these data demonstrate that the C3-PPIL1 association and inflammasome activation is critical for the induction of cell migration downstream of S1P/S1PR1 signaling.

To understand how S1P/S1PR1/AKT signaling induces C3 activation, we investigated whether cathepsin L (CTSL), a lysosomal cysteine protease, which was shown to mediate intracellular C3 complement activation,⁴⁴ is responsible for cleaving C3 into C3b- α' ₂ or C3a activation fragments to mediate cell migration and invasion. Interestingly, treatment of B16 cells with an irreversible inhibitor of CTSL in response to S1PR1 overexpression

attenuated cell migration (Figure S4A), and invasion (Figure S4B) compared with untreated control. This result was consistent with decreased intracellular C3 activation fragments and decreased levels of NLRP3, cleaved-IL-1 β , or active-caspase-1 compared with untreated controls (Figure S4C). In addition, inhibiting CTSL suppressed C3a secretion in cells that stably overexpress S1PR1 compared with controls (Figure S4D), supporting the role of CTSL in mediating intracellular C3 activation in response to S1P/S1PR1 signaling. Next, we assessed CTSL protein expression in cells stably transfected with S1PR1 for ectopic expression with/without CRISPR-Cas9-mediated silencing of PPIL1. CTSL expression was decreased in response to CRISPR-Cas9-mediated silencing of PPIL1 but CTSL protein levels were partially rescued in the S1PR1 overexpressing cells compared with vector-transfected control cells (Figure S4E). Inhibition of the CTSL expression in response to PPIL1 silencing is expected due to decreased NLRP3/inflammasome signaling, which in turn attenuates S1P/S1PR1 signaling because of their positive feedback signaling. In fact, addition of exogenous HDL-S1P to the PPIL1 knockout cells with/without S1PR1 overexpression significantly prevented CTSL expression compared with controls (Figure S4E). Interestingly, inhibiting AKT with MK-2206 2HCl prevented exogenous HDL-S1P-mediated rescue of the CTSL expression in PPIL1 knockout cells in the absence or presence of S1PR1 overexpression compared with controls (Figure S4E). Furthermore, the addition of exogenous HDL-S1P significantly protected p-AKT expression in PPIL1 knockout cells with/without S1PR1 overexpression compared with controls (Figures S4F and S4G). These data further support that S1P/S1PR1 signaling mediates p-AKT expression, leading to CTSL-mediated C3 cleavage/activation.

Conversely, C3b- α' ₂^{E156A} mutant expression and CRISPR-Cas9-mediated silencing of PPIL1 in S1PR1 overexpression cells did not have any effect on cathepsin B or cathepsin G proteases (Figure S4H), indicating the specificity of CTSL to mediate intracellular C3 activation. In addition, to further understand the role of CTSL in a metastatic cell line that does not require the forced expression of our proteins of interest, we utilized UM-SCC-22B cells derived from its parental UM-SCC-22A cells. Inhibiting CTSL in UM-SCC-22B cells decreased cell migration compared with untreated controls (Figure S4I). Moreover, CTSL expression is elevated in UM-SCC-22B at both protein (Figures S4J and S4K) and mRNA (Figure S4L) levels, which is consistent with the elevated S1PR1 mRNA levels (Figure S4L), compared with the parental UM-SCC-22A cells. We also observed that inhibiting S1PR1 with Ex26 and AKT with MK-2206 2HCl in UM-SCC-22B cells prevents CTSL expression at the protein levels compared with untreated control (Figure S4M). However, at the mRNA levels, AKT inhibition did not decrease CTSL or S1PR1 expression in UM-SCC-22B cells (Figure S4N). Together, these results suggest that intracellular C3 activation via generation of C3b- α' ₂ and C3a fragments downstream of S1P/S1PR1/AKT signaling is regulated by induction of CTSL protein levels to mediate cancer cell migration/invasion.

Effects of S1P/S1PR1/C3 signaling on lung colonization/metastasis *in vivo*

To delineate the effects of intracellular S1P and C3 on tumor metastasis *in vivo*, we injected B16 cells expressing various vectors (for S1PR1 overexpression or PPIL1 knockdown) into the tail vein of C57BL/6J mice and measured lung colonization and metastasis after 21 days. Induction of intracellular S1P signaling in B16 cells by treatment with JTE-013/DPO in

cell culture (before tail vein injections) or stably expressing S1PR1, highly increased lung colonization/metastasis compared with vehicle-treated and vector-only-transfected controls as detected by increased lung weight (Figures S5A and S5B), lung tissue area occupied by the tumor (Figure S5C), and total tumor nodules in the lungs (Figure S5D). To determine if intracellular S1P signaling induces lung metastasis by the C3-PPIL1 complex, we also injected B16 cells stably transfected with CRISPR-Cas9 vectors⁴⁵ to target PPIL1 with/without JTE-013/DPO exposure. These data showed that, although PPIL1 knockdown had no impact on lung metastasis, it largely inhibited lung colonization/metastasis in response to JTE-013/DPO-mediated S1P/C3 signaling (Figures S5A-S5D). Detection of C3-PPIL1 interaction in lung tissues of these mice using PLA showed that activation of the S1P/S1PR1/C3 signaling in response to JTE-013/DPO exposure or ectopic expression of S1PR1 resulted in ~30- to 40-fold induction compared with controls, which was blunted by PPIL1 knockdown (Figure S5E). We also measured cytokines and chemokines in the lung tissues of these mice using Eve Technologies' multiplex discovery assay probing 18 chemokines, cytokines, and growth factors. We found a massive induction in inflammatory cytokine levels, including IL-1 β , in response to JTE-013/DPO exposure or ectopic expression of S1PR1, which was also attenuated by PPIL1 knockdown compared with controls (Figure S5F). The alterations of IL-1 β in these lung tissues were also confirmed by western blotting (Figure S5G). *In situ* hybridization using RNA scope also showed that JTE-DPO exposure or WT-S1PR1 overexpression enhanced NLRP3 and C3aR1 expression in B16-derived lung metastasis and adjacent non-cancerous lung tissues, compared with vector-transfected and vehicle-treated controls (Figures S5H-S5J). Interestingly, S1P/S1PR1-mediated C3aR1 expression was induced mainly in the non-cancerous adjacent lung tissues (Figures S5I and S5J), whereas S1P/S1PR1-induced NLRP3 was detected mainly in the B16-derived metastatic lung tumors (Figure S5H). Also, JTE-DPO-mediated induction of C3aR1 and NLRP3 expression in the B16-derived lung metastasis and surrounding non-cancerous lung tissues were blunted by CRISPR-Cas9-mediated silencing of endogenous PPIL1 (Figures S5H-S5J). In addition, in lung tissues, C3a was significantly increased in mice injected with JTE-DPO-treated cells and S1PR1 overexpression cells, which was attenuated by PPIL1 knockdown (Figure S5K), suggesting a possible role of C3a-C3aR1 signaling in inducing tumor metastasis. Furthermore, RNA-seq data on mice lungs showed that injected S1PR1 overexpression cells in WT mice induced several complement-related genes, inflammasomes, and cell migration genes, including C3, C3ar1, Il1b, Nlrp3, Aim2, Il6, Ppil1, Vegf, and H-Ras, compared with vector-injected cells in WT mice (Figures S5L-S5N). Consistently, the expression of C3, C3ar1, IL-1 β , and Nlrp3 genes were confirmed with RNA scope *in situ* hybridization (Figures S5O-S5S). These data suggest that activation of the intracellular S1P/S1PR1/C3 signaling induces tumor metastasis controlled by the endogenous C3-PPIL1 complex, which is linked to the pro-inflammatory TME through inflammasome activation. These data also suggest that there might be crosstalk between tumor S1PR1 and systemic C3a-C3aR1 signaling that can play an additional role in inducing pro-inflammatory TME to enhance tumor metastasis.

To determine if C3a-C3aR1 signaling regulates S1PR1-induced lung colonization/metastasis, we measured the effects of C3aR1 genetic loss on lung colonization of B16-derived tumors with/without S1PR1 overexpression in WT or C3aR1^{-/-} mice. The tail vein

injection of B16-derived tumors expressing S1PR1 in WT mice resulted in the exacerbation of lung metastasis, which was primarily prevented in C3aR1^{-/-} knockout mice compared with vector-only-transfected B16-derived tumors (Figures 6A and 6B). In the lung tissues, lipidomics analyses indicated a significant increase of S1P levels in WT mice injected with S1PR1 overexpression cells compared with WT mice injected with vector control cells but insignificant compared with C3aR1^{-/-} knockout mice (Figure 6C, left panel). Moreover, in the serum, we detected an increase in S1P levels using lipidomics in WT mice injected with S1PR1 overexpression cells compared with WT mice injected with vector control cells or C3aR1^{-/-} knockout mice (Figure 6C, right panel). To confirm the extent of tumors colonized to the lungs, we utilized p63 and Ki-67 cell proliferation markers. Both p63 (Figures 6D and 6E) and Ki-67 (Figures 6F and 6G) levels were significantly increased in WT mice injected with S1PR1 overexpression cells compared with WT vector or C3aR1^{-/-} mice. In addition, our RNA scope *in situ* hybridization data showed that S1PR1 overexpression injected cells significantly induced C3, NLRP3, and IL-1 β mRNAs in B16-derived metastatic lung tumors and adjacent lung tissues of WT mice, but not in C3aR1^{-/-} knockout mice (Figures 6H-6J). Overall, these data support that genetic silencing of systemic complement receptor (C3aR) signaling attenuates S1PR1-mediated tumor metastasis, consistent with the inhibition of NLRP3-mediated inflammasome and IL-1 β signaling.

The S1P/complement crosstalk plays a critical role in the regulation of overall survival in cancer patients

To examine the clinical relevance of the S1P/S1PR1/C3 axis, we obtained metastatic breast tumor tissues from the lungs of three ER⁺ breast cancer patient-derived xenograft models⁴⁶ versus three patient's benign breast tumors. Three metastatic breast tumors highly expressed S1PR1 and C3, which were consistent with overexpression of NLRP3, cleaved-IL-1 β , and active-caspase-1 compared with benign tumors (Figure S6A). We also performed RNA scope *in situ* hybridization using skin tissues at different stages of melanoma (normal skin tissue, benign tumor, malignant tumor, and metastatic tumor) to measure the expression of C3 and S1PR1. The data showed that expression of C3 and S1PR1 is increased in tumor tissues obtained from patients with metastatic melanoma, compared with local tumors, as measured using *in situ* hybridization and RNA scope (Figures S6B and S6C). Moreover, TCGA analyses showed that overexpression of S1PR1, C3, PPIL1, and NLRP3 is associated with poor survival of patients with all the 33 combined cancer types available in the TCGA database (Figure S6D). Specifically, in uveal melanoma, the most common primary and deadly intraocular malignancy,⁴⁷ is associated with poor patient survival when S1PR1-C3-PPIL1-NLRP3 are overexpressed (Figure S6E), supporting the clinical relevance of S1P/S1PR1/C3 signaling in metastatic tumors.

Pharmacologic targeting of C3 and NLRP-mediated inflammasome attenuate C3-mediated tumor metastasis *in vivo*

Our studies suggest that C3 and NLRP3-dependent inflammasome signaling provide valuable targets to inhibit tumor metastasis. To test this, we generated B16-derived xenografts transfected with vector-only control plasmids, or WT-C3b- α '₂ and mutant-C3b- α '₂ with E156A conversion that did not bind PPIL1. We measured their growth in the absence/presence of MCC950 (NLRP3 inhibitor) or CR2-Crry (C3 inhibitor) in C57BL/6J

mice. Ectopic expression of WT-C3b- $\alpha'2$, but not the E156A-C3b- $\alpha'2$ mutant, increased lung metastasis compared with vector-only-transfected controls, as seen by increased lung weight (Figure 7A), tumor p63 (Figures 7B and 7C), and Ki-67 (Figures 7D and 7E) levels. Inhibition of NLRP3-inflammasome or C3 complement signaling using MCC950 or CR2-Crry, respectively, almost completely abrogated lung metastasis of WT-C3b- $\alpha'2$ -expressing xenograft-derived tumors compared with tumors expressing the E156A-C3b- $\alpha'2$ mutant or vector-transfected controls (Figures 7A-7E). After treatments were completed, metastatic lungs were surgically removed from mice, and we performed *in situ* hybridization using RNA scope to measure the expression of NLRP3 and IL-1 β . Ectopic expression of the WT-C3b- $\alpha'2$ but not the mutant E156A-C3b- $\alpha'2$ resulted in enhanced expression of NLRP3 (Figure 7F) and IL-1 β (Figures 7G and 7H) in metastatic lung tumors overexpressing WT-C3b- $\alpha'2$ but not the mutant E156A-C3b- $\alpha'2$. Significantly, inhibition of NLRP3/inflammasome or C3 signaling using MCC950 or CR2-Crry, respectively, blunted the effects of WT-C3b- $\alpha'2$ on overexpression of NLRP3 and IL-1 β in metastatic lung tumors compared with vehicle-treated controls (Figures 7F-7H). These data suggest that pharmacologic targeting of NLRP3/inflammasome and C3 signaling provide new strategies to attenuate S1P/S1PR1/C3/inflammasome-mediated tumor metastasis.

Also, we injected luciferase-expressing MDA231-LM2-4175 (LM2-4/Luc+) cells into the mammary fat pad of Balb/c nude mice. When the primary mammary tumors reached 100 mm³, the mice were randomly placed into two groups and treated with either MCC950 and CR2-Crry or vehicle-treated controls. After 6 weeks of treatment, we observed that the MCC950 + CR2-Crry combination delays primary tumor growth as demonstrated by the luciferase intensity in tumors (Figure S7A) and tumor volumes (Figures S7B and S7C) compared with the untreated control mice. More importantly, in our *ex vivo* imaging to detect luciferase presence in the lungs and liver, we observed 0% liver and lung metastasis in the MCC950 + CR2-Crry-treated mice, compared with 37.5% liver and lung metastasis presence in the control mice (Figure S7D and S7E), suggesting the significance of targeting NLRP3 and C3 complement as a therapeutic strategy to attenuate tumor growth and metastasis. Inhibition of NLRP3-inflammasome and C3 activation using MCC950 + CR2-Crry significantly decreased C3a levels in the isolated primary tumors and serum but remained unchanged in lungs compared with control mice (Figure S7F), which confirms the inhibition of C3 activation. In addition, MCC950 + CR2-Crry decreased S1P levels in the serum, while its levels remained unchanged in the tumors compared with controls (Figure S7G). Interestingly, in the tumors isolated from mice treated with MCC950 + CR2-Crry, S1PR1, C3, and NLRP3 inflammasome proteins were decreased compared with control mice (Figures S7H and S7I). At the mRNA level, MCC950 + CR2-Crry decreases NLRP3 and IL-1 β expressions compared with control mice (Figure S7J), supporting the inhibition of NLRP3 inflammasome. Although S1PR1 levels also seemed to be decreasing at the mRNA levels, the decrease was insignificant (Figure S7J). These data suggest a positive feedback loop mechanism between downstream NLRP3-inflammasome and S1PR1 signaling in metastatic tumors *in vivo*. Conversely, in the non-tumorigenic lungs, MCC950 + CR2-Crry treatment did not significantly affect S1PR1, C3, or NLRP3-inflammasome proteins, compared with control mice (Figures S7K and S7L). Consistent with our cell culture results, in our PLA experiment, MCC950 + CR2-Crry treatment inhibited C3-PP1L1

binding in the tumors compared with control mice tumors *in vivo* (Figures S7M and S7N). On the contrary, MCC950 + CR2-Crry did not significantly affect C3-PPIL1 binding in non-tumorigenic lungs compared with control mice (Figure S7O). Thus, our data suggest that the pharmacologic targeting of NLRP3/inflammasome and C3 signaling provides a new strategy to prevent tumor growth and metastasis *in vivo*.

DISCUSSION

In this work, we set out experiments to understand the link between S1P metabolism and complement signaling for the induction of tumor metastasis. Data presented here support the role of the S1P/S1PR1 and C3/PPIL1 axis in cancer cells and in the TME to induce tumor metastasis by facilitating pro-inflammation/inflammasome signaling. In addition, our data also demonstrate that HDL-bound S1P enhanced cancer cell migration more than BSA-bound S1P, which is consistent with a previous study that showed a selective role of HDL-ApoM-bound S1P in the regulation of lymphopoiesis and neuroinflammation.⁴

Metastasis has been associated with cancer cell-induced changes in the TME, presenting another layer of complexity to cancer as a systemic disease.^{1,2} However, how cancer cells induce changes within the TME and how these systemic changes regulate cell-to-cell interactions between cancer and immune cells, such as macrophages, myeloid-derived suppressor cells, natural killer cells, neutrophils, or cytotoxic CD8⁺ and CD4⁺ T cells,²⁹ to regulate tumor metastasis remain enigmatic. In the past several decades, cancer research studies largely ignored the importance of the immune components' roles in regulating tumor growth/progression and response to therapy. Recent basic and clinical research demonstrated that cancer therapy's complexity arises partly from integrated signaling pathways that play vital roles in regulating cancer and immune cell functions involved in innate or adaptive immunity. Our data demonstrate a new mechanism that regulates cell-to-cell communication within the TME via crosstalk between S1P and complement signaling to enhance cancer cell migration and metastasis.

The complement system is a critical component of the innate immune system that eliminates pathogens, primes the adaptive immune response, and clears apoptotic cells and immune complexes.⁴⁸⁻⁵⁰ Until recently, it was generally accepted that the complement system played a role in tumor surveillance and tumor killing. However, the efficacy of complement-mediated killing was relatively poor unless supplemented with exogenous anti-tumor monoclonal antibodies.⁵¹⁻⁵³ Recent studies suggest that tumor cells can subvert complement system components to promote tumorigenesis in a shift from this well-held paradigm. Several studies have now demonstrated that complement molecules, such as C3a/C5a, the anaphylatoxin cleavage fragments, can be produced by tumor cells and utilized to promote angiogenesis, metastasis, and immunosuppression leading to enhanced tumor survival.⁵⁴⁻⁵⁸ Interestingly, in addition to the activation of C3b- α '₂, we also observed secretion of C3a in response to S1P/S1PR1 signaling, which seemed to be dependent on CTSL expression and activity. Our data suggest that, while C3b- α '₂ associates with PPIL1 to activate the inflammasome in tumors to induce metastasis, secreted C3a from tumors can associate with C3aR1 in the TME to exacerbate lung colonization and metastasis. This was supported by reduced lung metastasis in response to systemic knockout of C3aR1 in our study, which

was associated with decreased systemic S1P, and attenuation of C3, NLRP3 and IL-1 β expression in metastasized tumors in the lungs, suggesting that C3a/C3aR1 signaling in the TME could regulate tumor metastasis via elevating systemic S1P which then activates the S1PR1/C3/NLRP3/IL-1 β signaling axis in cancer cells as described here. However, silencing S1PR1, or inhibition of inflammasome in combination with C3 activation using pharmacological inhibitors, largely prevented lung colonization in tail-vein-injected B16 melanoma cells in C57BL/6J mice. Similarly, pharmacologic inhibition of inflammasome and C3 activation suppressed the primary mammary tumor growth and lung metastasis after mammary pad injection of breast cancer cells in nude mice. Overall, these data reveal a new mechanism whereby endogenous S1P via paracrine and/or autocrine S1PR1 signaling induces complement C3 activation in cancer cells, which mediates intracellular C3b- α' ₂-PPIL1 complex formation and metastatic NLRP3-dependent inflammasome signaling. Thus, the pro-metastatic S1PR1/C3/NLRP3 signaling provides a target to inhibit tumor growth and metastasis *in vivo*.

Limitations of the study

Some challenges need to be addressed in future studies. For example, the precise mechanism by which S1P/S1PR1 activates C3/complement remains unknown. Although our preliminary data suggest that p-AKT activation and CTSL-mediated C3 cleavage is involved in this process, it is still unknown how the S1P/S1PR1/AKT signaling activates CTSL in cancer cells. However, roles of CTSL activation in C3 activation and metastasis induction is consistent with previously published data.^{44,59-61} Another question that remained unanswered is the function of PPIL1 and the C3/PPIL1 complex to mediate NLRP3/inflammasome activation. PPIL1 regulates protein phosphorylation and RNA splicing.^{62,63} Therefore, it needs to be explored whether PPIL1 controls C3 activation by inducing its phosphorylation and regulates inflammasome-related gene expression by controlling the splicing machinery. Moreover, although our studies demonstrated that S1P/S1PR1 activates intracellular C3/complement signaling through its PPIL1 complex formation, the fact that C3aR1^{-/-} mice were protected from B16-derived tumor metastasis in response to S1PR1 activation also suggests that there is a systemic role of C3a/C3aR1 signaling, which induces systemic S1P that activates the S1PR1/C3/NLRP3/IL-1 β in cancer cells to enhance lung colonization/metastasis. However, how systemic C3a/C3aR1 signaling is activated in TME, which cells are involved in C3a/C3aR1-mediated signaling in the TME, and the mechanisms of C3a/C3aR1-dependent systemic S1P regulation need to be determined. Nevertheless, activation of the NLRP3/IL-1 β /inflammasome by C3a or C5a signaling in monocytes and CD4⁺ T cells is consistent with our data.^{64,65}

Thus, our data suggest that induction of the S1P/S1PR1/C3 axis induces cancer cell migration via inflammasome activation, which involves NLRP3, caspase-1, and IL-1 β -mediated proinflammation. These data also provide a mechanism-based strategy to target the S1PR1/C3 crosstalk and NLRP3/inflammasome signaling to attenuate tumor metastasis.

STAR★METHODS

RESOURCE AVAILABILITY

Lead contact—Further information and requests for resources and reagents should be directed to and will be fulfilled by the Lead Contact, Besim Ogretmen (ogretmen@musc.edu).

Materials availability—All unique/stable reagents generated in this study are available from the Lead contact with a completed Materials Transfer Agreement.

Data and code availability

- The RNA sequencing data generated during this study have been deposited at Gene Expression Omnibus (GEO) under the accession numbers GSE172156 and GSE169443. Original, uncropped western blot image files have been deposited at Mendeley Data and are publicly available as of the date of publication, V1, <https://doi.org/10.17632/3g49sgnbt.1>.
- This paper does not report original code.
- Any additional information required to reanalyze the data reported in this paper is available from the lead contact upon request.

EXPERIMENTAL MODEL AND SUBJECT DETAILS

Human tissues and tumor microarray analyses (TMA)—TMA slides that include normal tissues, benign tumors, malignant, and metastatic malignant melanoma tissues were purchased from US Biomax, Inc (Rockville, MD, USA) and prep for RNA scope experiment. Briefly, slides were baked for 1hr at 60°C and placed into xylene and ethanol for de-paraffinization and rehydration, followed by hydrogen peroxide, antigen retrieval, and protease plus steps. Then, hs-C3 (ACD, cat#430701) and Hs-S1PR1 (ACD, cat#491201) dual detection probes were conducted using RNAscope 2.5 HD Duplex Reagent Kit-Hs (ACD, cat#322435), according to the manufacturer's instructions.

GEPIA2 and TCGA analyses—Survival analysis was conducted using GEPIA2 (<http://gepia2.cancer-pku.cn/#survival>) default settings under Expression Analysis functions with 50% low and high cut-offs and 95% confidence intervals.

Patient-derived xenografts (PDX)—The ER+ PDX models were established from metastatic bone biopsies of ER+ breast cancer patients progressing on endocrine therapy.⁴⁶ PDX tumors were implanted in the neck region of nu/nu mice, and mice were given estradiol supplementation in drinking water. When the tumors reached the ethical size cut-off, mice were sacrificed, and tumor pieces were collected for downstream analysis. These experiments have been approved by the Institutional Animal Care and Use Committee of the University of South Carolina. All mice were maintained under a temperature-controlled environment with a 12 h light/dark cycle and received a standard diet and water ad libitum.

Animal studies—All animal experiments were performed under protocols approved by the Institutional Animal Care and Use Committee (IACUC) at the Medical University of South Carolina (MUSC). Female C57BL/6J mice were purchased from The Jackson Laboratory (cat# 000664). Male and female C3aR1^{-/-} knockout mice were obtained from Dr. Carl Atkinson's group (MUSC and currently at the University of Florida). All transfected or drug-treated B16-F10 mouse melanoma cells were harvested by trypsinization, washed in PBS, counted, and resuspended in serum-free RPMI media for tail vein metastasis assays. Female C57BL/6J or C3aR1^{-/-} mice (6–8 weeks-old) were anesthetized and 25×10^4 cells (100 μ L) injected into the tail vein with sterile BD Micro-Fine™ IV Insulin Syringes (Fisher Scientific, cat#14-829-1B). Alcohol pads and heat lamps were also used for tail vein visibility. Mice were sacrificed after 21 days, and lungs were isolated for metastasis analysis. To determine the role of C3 and NLRP3 in tumor metastasis, female C57BL/6J mice were injected intraperitoneally (i.p.) with 20 mg/kg MCC950 Sodium (Selleckchem, cat#S7809) or vehicle control (PBS) every second day for 7 days before tail vein injection of cells, and every second day for 21 days after tail vein injection. Another group of female C57BL/6J mice was injected i.p. with 10 mg/kg of mouse complement inhibitor CR2-Crry or vehicle control (PBS) every second day for 21 days after tail vein injection. For the spontaneous metastasis experiment, luciferases expressing MDA231-LM2-4175 (LM2-4/Luc+) cells were harvested by trypsinization, washed in PBS, counted, and resuspended in a 1:1 solution of 1X PBS and Geltrex Basement Membrane Matrix. One million LM2-4/Luc + cells (100 μ L) were injected into the fifth inguinal mammary fat pad of female Balb/c nude mice (8-9 weeks-old). The primary tumor growth was monitored weekly by measuring the tumor length and width with a digital caliper. Tumor volumes were calculated as $\frac{1}{2} (\text{Length} \times \text{Width}^2)$. When tumors reached 100mm³ mice were randomly placed in two groups, the CR2-Crry + MCC950 group and the untreated control group. CR2-Crry (10 mg/kg) and MCC950 (20 mg/kg) were given i.p. every second day for 6 weeks. To monitor *in vivo* tumor progression, mice were anesthetized and injected i.p. with 150 mg/kg D-luciferin (Selleckchem, cat# S7763). Imaging was done after 10mins of D-luciferin injection using PerkinElmer Maestro 2 in-vivo imaging system with Low Light acquisition. Luciferase intensity in tumors was quantified using Maestro 2 analysis software. For *ex vivo* imaging, mice were anesthetized and injected i.p. with 150 mg/kg D-luciferin just before euthanasia. After necropsy, liver and lung tissues were individually placed on a 24-well plate, and 0.3mg/mL D-luciferin solution was added to cover the tissues completely. Tissues were then imaged using PerkinElmer Maestro 2 imaging system.

***In vivo* detection of lung metastasis in mice**—Lung tissues were immediately harvested after euthanasia, fixed in 10% formalin solution for 24 h at room temperature, and transferred to 70% room temperature ethanol. Tissues were processed, and 200 μ m Sections were cut and trimmed to prepare hematoxylin & eosin (H&E), and immunohistochemistry (IHC) slides. The H&E slides were assessed for tumor metastasis by a pathologist.

Cell lines and culture conditions—B16-F10 (ATCC® CRL-6475™) was cultured in Roswell Park Memorial Institute (RPMI) 1640 Medium, while 4T1 (ATCC® CRL-2539™), MyC-CaP (ATCC® CRL-3255™), 293T (ATCC® CRL-3216™), MB49, UM-SCC-22A,

UM-SCC-22B, MDA-MB-231, LM2-4175, and BOM-1833 cell lines cultured in Dulbecco's Modified Eagle Medium (DMEM) and incubated at 37°C in 5% CO₂ atmosphere. Both RPMI and DMEM media were supplemented with 10% fetal bovine serum (FBS), 1% penicillin-streptomycin(100x), and 0.2% of 2.5 mg/mL Plasmocin™ Prophylactic (InvivoGen, cat# ant-mpp). Cells were passaged around 80-90% confluency using 0.05% trypsin-0.02% EDTA solution followed by 1000rpm centrifugation for 5mins. Trypan Blue solution (Millipore Sigma, cat# T8154) and MTT Cell Proliferation Assay (ATCC® 30-1010K) were used to determine cell viability and were appropriate. The MDA-MB-231, LM2-4175, and BOM-1833 progression series cell lines were obtained from Dr. Philip Howe's group (MUSC).

METHOD DETAILS

Boyden chamber assay—Twenty-four wells of falcon cell culture inserts (cat# 353097) with 8.0-micron pore size were pre-coated with 50µg/mL fibronectin (Corning inc. cat# 354008) at 37°C for 30mins before seeding cells. First, 5×10^4 cells were seeded in the upper chamber of the trans-well insert with serum-free media. The lower chamber contained 10% FBS media as the chemoattractant, and the cells were incubated at 37°C for 24 h in a CO₂ incubator. After incubation, cells were washed with 1X PBS pH 7.4 (cat# 10010-023) and fixed with 4% PFA (Boster, cat# AR1068) for 15mins. Next, non-migrated cells in the upper chamber were washed away with 1X PBS and removed with a cotton-tipped application (VWR, cat# 89031-270). Next, migrated cells in the lower chamber were stained with 0.5% crystal violet in 2% methanol solution for 15mins at room temperature. After staining, the cells were washed, and the lower chamber membrane with cells was removed from the insert, transferred into a 96-well plate, and lysed with 10% acetic acid (Fisher Scientific, cat# 135-32) before using a microplate reader to measure optical density at 630nm for migration quantification. Representative images were taken with an Olympus CKX41 bright field microscope. All migration assay experiments were done alongside MTT Cell Proliferation Assay (ATCC, cat# 30-1010K), which was used as normalization to produce the final migration datasets. For cell invasion assays, the CytoSelect™ 24-Well Cell Invasion Assay and Basement Membrane kit from Cell Biolabs, Inc (Cat# CBA-110) were used according to the manufacturer's instructions.

Wound healing assay—CytoSelect™ 24-Well Wound Healing Assay kit from Cell Biolabs, Inc (Cat# CBA-120) was used according to the manufacturer's instructions. Wound recovery was determined using ImageJ software to calculate percent migration with the formula $(1 - (\text{area after 24 h} / \text{area at 0 h})) \times 100\%$ since the cells were fixed and stained at 0 and 24 h after removal of the inserts. Representative images were taken with an Olympus CKX41 bright field microscope.

Antibodies—The antibodies used in this study, including their unique identifiers, are listed in the key resources table.

Pharmacological inhibitors—The pharmacological inhibitors used were as follows; JTE-013 used at 1µM (Cayman, cat# 10009458), 4-deoxy Pyridoxine (DPO) used at 5mM (Cayman, cat# 21863), Ex 26 used at 5nM (Tocris, cat# 5833), MK-2206 2HCl used at

1 μ M (Selleckchem, cat# S1078), MCC950 used at 10 μ M (Selleckchem, cat# S8930), and Cathepsin-L inhibitor used at 10 μ M (Enzo Life Sciences, Inc., Cat# ALX-260-134-M001). Cells were treated in serum-free media. In addition, CR2-Crry was obtained from Dr. Stephen Tomlinson's group (MUSC).

Western blotting—Cells and tissues were lysed in Pierce RIPA buffer (Thermo Fisher Scientific, cat# 89900) supplemented with 1M DTT (Cell Signaling, cat# 7016L), Protease Inhibitor Cocktail (Sigma-Aldrich, cat# P8340), and PMSF Protease Inhibitor (Thermo Fisher Scientific, cat# 36978). Proteins were resolved by SDS-PAGE, transferred to PVDF membrane, and immunoblotted with corresponding antibodies. SuperSignal™ West Pico PLUS Chemiluminescent Substrate (Thermo Fisher Scientific, cat# 34580) or Clarity Max Western ECL Substrate (Bio-Rad, cat # 1705062) and ChemiDoc imaging system were used for blot detection.

Co-immunoprecipitation—Cells were lysed in Pierce IP Lysis Buffer (Thermo Fisher Scientific, cat# 87787) supplemented with 1M DTT (Cell Signaling, cat# 7016L), Protease Inhibitor Cocktail (Sigma-Aldrich, cat# P8340), Phosphatase Inhibitor (ThermoFisher Scientific, cat# 78428), and PMSF Protease Inhibitor (Thermo Fisher Scientific, cat# 36978). Magnetic SureBeads protein A or G (Bio-Rad, cat#1614833) were used for pull-down, according to the manufacturer's instructions, with minor modifications. Proteins were resolved by SDS-PAGE, transferred to PVDF membrane, and immunoblotted with corresponding antibodies before detection via chemiluminescence as above.

Proteomics—Co-immunoprecipitation (co-IP) with anti-C3 antibody or IgG as a negative control, followed by SDS-PAGE and Coomassie staining (Bio-Rad, cat #1610786), were performed. Gel lanes for individual samples were cut out, put in 1.5mL Eppendorf tubes with molecular grade water, and sent to The Harvard Taplin Biological Mass Spectrometry Facility for proteomics analysis.

Biomolecular docking simulations—We probed the possible interaction of C3b- α' ₂ with PPIL1 using biomolecular docking of X-ray derived protein structures. First, a C3b- α' ₂ homology model was built using MOE software and CCC3 pdb:2A73 (PMID 16177781) as a template. This model then interacted with PPIL1 pdb:2X7K (PMID 20368803) for biomolecular docking using the docking server ClusPro.⁶⁶ The top 10 lowest energy models were then analyzed for interacting residues.

Proximity ligation assay (PLA)—Cells were fixed in 4-well chamber slides (Fisher Scientific, cat# 154526) with 4% PFA (Boster, cat# AR1068) and permeabilized with 0.1% IGEPAL in 1XPBS. Formalin-fixed paraffin-embedded (FFPE) tissue samples were deparaffinized and rehydrated before heat-induced epitope retrieval using antigen unmasking solution (Vector laboratories, cat# H-3300). PLA was performed using Duolink *in situ* hybridization (Sigma-Aldrich, cat# DUO92101), and experimental procedures were done according to the manufacturer's instructions. PLA images were quantified using Duolink Image Tool Software (Olink Bioscience).

Plasmids and shRNAs—Lentivirus was produced into 293T cells by transfection using the Applied Biological Materials Inc. (ABM) 's second Gen. Packaging Mix & Lentifectin Combo Pack (cat# LV003-G074). After 24 h, viral particles were collected, centrifuged (15mins, 1300rpm), and filtered with a 0.45µm filter. Then, the viral particles were added to the cells of interest for 48 h with 8µg/mL polybrene. Puromycin (InvivoGen, cat#ant-pr-1) or G418 (InvivoGen, cat#ant-gn-1) was used to create stable transfection cell lines.

The following expression and mutagenesis plasmids were synthesized/purchased from Genscript Biotech.

Mouse S1pr1(NM_007901.5) ORF Clone, pcDNA3.1+/C-(K) DYK (Cat# OMu20424D)

Mutagenesis: S1pr1 R120A, pcDNA3.1+/C-(K)DYK.

Mutagenesis: S1pr1 W269L, pcDNA3.1+/C-(K)DYK.

Express Cloning: C3b alpha 2 prime (C3b-α^{'2}) _pcDNA3.1(+)-C-DYK.

Mutagenesis: Mut#1: C3b-α^{'2} D111A, pcDNA3.1(+)-C-DYK.

Mutagenesis: Mut#2: C3b-α^{'2} E156A, pcDNA3.1(+)-C-DYK.

Mutagenesis:2xMut: C3b-α^{'2} D111A, E156A, pcDNA3.1(+)-C-DYK.

The following CRISPR lentiviral vectors were purchased from Applied Biological Materials Inc.

Ppil1 sgRNA CRISPR All-in-One Lentivirus set (Mouse), NM_026845.4 (cat# 3736711 and cat# 373671140502)

CRISPR Scrambled sgRNA All-in-One Lentiviral Vector (with spCas9)- (cat# K010)

The following shRNA constructs were purchased from Sigma Aldrich.

Complement component 3 MISSION shRNA Plasmid
DNA (cat# SHCLND-NM_009778) (Sequence:CCGGCCATCAAGAT
TCCAGCCAGTACTCGAGTACTGGCTGGAATCTTGATGGTTTTTG)

Sphingosine-1-phosphate lyase 1 (SGPL1) MISSION shRNA
Plasmid DNA (cat#SHCLND-NM_009163) (Sequence:CCGGG
ATCGAACAAACAGGTGAGCAACTCGAGTTGCTCACCTGTTGTTTCGATCTTTTTTG)

MISSION[®] pLKO.1-puro non-Target shRNA Control Plasmid DNA (cat# SHC016).

Primers and q-RT-PCR—Total RNA was isolated using QIAzol Lysis Reagent (Qiagen, cat# 79306), and 1µg extracted RNA was reverse transcribed using iScript cDNA Synthesis Kit (Bio-Rad, cat#1708891). SsoAdvanced Universal SYBR Green Supermix (Bio-Rad cat# 1725271) was used for q-RT-PCR. In addition, 18S ribosomal RNA or β-actin was used for internal control and data normalization. All procedures were done according

to the manufacturer's instructions. All q-RT-PCR primers were synthesized by Integrated DNA Technology (Iowa, USA). The specific q-RT-PCR primers designed are listed in key resources table.

Exogenous S1P exposure—1 mg of S1P was resuspended in 100% methanol: molecular lab grade water in the ratio 95:5 and sonicated in a bath sonicator for about 10 min. 1 μ L of 10M HCl was added for complete resuspension. Resuspended S1P in a glass tube was dried entirely with a stream of nitrogen and stored at -20°C . Before treatment, dried S1P was resuspended in BSA (Free Fatty acid BSA) or HDL (High-Density Lipoprotein) for BSA-S1P or HDL-S1P conjugation, respectively, and incubated at 37°C for 30 min.

RNA-sequencing—Total RNA was isolated using QIAzol Lysis Reagent (Qiagen, cat# 79306) and processed as per the manufacturer's instructions. Sample quality control, RNA library preparation (standard Illumina protocols), and RNA seq analysis were carried out by Novogene Corporation Inc. (Sacramento, CA 95826)

Cytokine measurements—Cytokine production in mice lungs was measured using protein lysates. Eighteen cytokine/chemokine/growth factor biomarkers (Mouse High Sensitivity T cell Discovery Array 18-Plex) were quantified at Eve Technologies Corp (Calgary, AB, Canada). The 18 cytokines/chemokines consisted of GM-CSF, IFN γ , IL-1 α , IL-1 β , IL-2, IL-4, IL-5, IL-6, IL-7, IL-10, IL-12 (p70), IL-13, IL-17A, KC/CXCL1, LIX, MCP-1, MIP-2, TNF- α . The sensitivities range from 0.06–9.06 pg/mL. Detail assay protocols or individual analyte values are available on Eve Technologies' website or in the Milliplex protocol.

Lipidomics analysis—For endogenous analyses of bioactive sphingolipids, mice tissues were lysed in RIPA buffer for protein extraction, and cell lines were first washed in 1X PBS before collecting cell pellets to determine their bioactive sphingolipid levels. Protein concentration (pmol/g protein) was used to normalize tissue lipid levels, while the total cell numbers were used for cell pellet lipid normalization. For cell culture media and mice serum lipid analyses, equal volumes were used to determine bioactive sphingolipid levels. The LC/MS/MS-based lipidomics at MUSC was used to perform all sphingolipid measurements.^{37,38}

Flow cytometry— 1×10^6 cells were resuspended in 1XPBS and centrifuged at 4°C , 1500rpm for 5mins. Staining was performed by incubating cells with the antibody at 1:10 dilutions in FACS buffer (1% BSA and 0.05% sodium azide in 1XPBS) for 30 min at 4°C in the dark, followed by centrifugation at 4°C , 1500rpm for 5mins. Cells were resuspended, washed in FACS buffer, and transferred to FACS tubes. For full expressions, fixation/permeabilization (BD Cytofix/Cytoperm Kit, BD Biosciences, San Jose, CA) was performed before staining. Samples were acquired on LSR Fortessa/X-20 and analyzed with FlowJo software (Tree Star, OR).

ELISA—PierceTM 96-Well Polystyrene Plate (Thermo Fisher Scientific, cat# 15042) was coated with primary antibody diluted at 1:300 in 1XPBS and incubated for 24 h at 4°C . Blocking was done for 3 h at room temperature in blocking buffer (2% BSA in 0.1%

PBST), followed by washing in 0.1% PBST. Cell supernatants were added to wells and incubated for 24 h at 37°C. HRP secondary antibody was used at 1:4000 diluted in blocking buffer and incubated at room temperature for 1 h, followed by washing and the addition of SuperSignal™ ELISA Femto Substrate (Thermo Fisher Scientific, cat# 37075) at a 1:1 ratio. The plate was then incubated in the dark for 10mins and analyzed using a microplate reader. The mouse C3a (Complement Component C3a) ELISA kit from MyBioSource, Inc. (Cat# MBS2506255) was used according to the manufacturer's instructions.

Immunohistochemistry (IHC)—FFPE slides were deparaffinized and rehydrated through a series of xylene and ethanol washes. Heat-induced epitope retrieval was performed for 30 min at 95°C. After primary and secondary antibody incubations, horseradish peroxidase (HRP)-chromogen detection was performed, followed by hematoxylin as a counter-staining.

In situ hybridization and RNA scope—Slides were baked in ACD HybEZ II Hybridization System (ACD, cat# 321710) for 1hr at 60°C and placed into fresh xylene and ethanol steps for de-paraffinization and rehydration. RNAscope Hydrogen Peroxide (ACD, cat#322335) was added for 10 min at room temperature, followed by 15mins target retrieval (ACD, cat#322000) at 100°C, and RNA scope protease plus (ACD, cat# 322331) for 30mins at 40°C. The RNAscope Detection Kits (ACD, cat# 322360) were used according to the manufacturer's instructions (Advanced Cell Diagnostics (ACD), Newark, CA, USA). The manufacturer's recommended control probes (positive and negative) were used for each experiment, as instructed. The list of ACD's probes used are as follows; Mm-C3ar1 (cat#476751), Mm-S1pr1 (cat# 426001), Mm-C3 (cat#417841), Mm-II1b (cat#316891), and Mm-Nlrp3 (cat# 439571).

QUANTIFICATION AND STATISTICAL ANALYSIS

RNA scope and IHC quantifications—The whole slide was scanned at 20X magnification using Akoya Vectra® Polaris™ Automated Quantitative Pathology Imaging System (Akoya Biosciences, Marlborough, MA). Tissue segmentation and cell phenotyping were performed using inForm® Software v2.4.10 (Akoya Biosciences, Marlborough, MA). The resulting image analysis was exported for further analysis. Cell counting and spatial analyses were performed using the PhenoptrReports Open-Source R Package (<https://akoyabio.github.io/phenoptrReports/index.html>, Akoya Biosciences, Marlborough, MA).

Statistical analyses—All data are presented as means ± SD (Standard Deviation) of at least three independent studies (n = 3). Group comparisons were performed with either two-tailed unpaired t-tests (and nonparametric tests) or a one-way ANOVA (and nonparametric or mixed) using Graph Pad Prism. In animal studies, the Kruskal-Wallis test was used to compare continuous outcomes among three groups due to relatively smaller sample sizes. Because a significant result was discovered, all possible pairwise comparisons were performed using the Wilcoxon rank-sum test. p < 0.05 (*) was considered significant. For clinical analyses, the significance was calculated by the Log rank test. For correlation analysis, Pearson correlation coefficients were calculated using GraphPad Prism Software, 8.0.1.

Supplementary Material

Refer to Web version on PubMed Central for supplementary material.

ACKNOWLEDGMENTS

We thank the members of the Ogretmen Laboratory for their technical support and helpful discussions. This work was supported by research funding from the National Institutes of Health (AG069769, CA214461, CA214461-S1, DE016572, and P01 CA203628) and the National Institute of General Medical Sciences (NIGMS) T32 training grant (T32GM132055). The core facilities utilized are supported by NIH (C06 RR015455), Hollings Cancer Center Support grant (P30 CA138313), or Center of Biomedical Research Excellence (Cobre) in Lipidomics and Pathobiology (P30 GM103339). In addition, the Zeiss 880 microscope was funded by a Shared Instrumentation grant (S10 OD018113). This study was performed in accordance with the guidelines in the Guide for the Care and the Use of Laboratory Animals of the National Institutes of Health. All the animals were handled according to the approved Institutional Animal Care and Use Committee (IACUC) protocol (2018-00412) of the Medical University of South Carolina.

INCLUSION AND DIVERSITY

We worked to ensure sex balance in the selection of non-human subjects. One or more of the authors of this paper self-identifies as an underrepresented ethnic minority in science. One or more of the authors of this paper received support from a program designed to increase minority representation in science.

REFERENCES

1. Klein CA (2009). Parallel progression of primary tumours and metastases. *Nat. Rev. Cancer* 9, 302–312. [PubMed: 19308069]
2. Ramel D, Wang X, Laflamme C, Montell DJ, and Emery G (2013). Rab11 regulates cell–cell communication during collective cell movements. *Nat. Cell Biol* 15, 317–324. [PubMed: 23376974]
3. Alvarez SE, Harikumar KB, Hait NC, Allegood J, Strub GM, Kim EY, Maceyka M, Jiang H, Luo C, Kordula T, et al. (2010). Sphingosine-1-phosphate is a missing cofactor for the E3 ubiquitin ligase TRAF2. *Nature* 465, 1084–1088. [PubMed: 20577214]
4. Blaho VA, Galvani S, Engelbrecht E, Liu C, Swendeman SL, Kono M, Proia RL, Steinman L, Han MH, and Hla T (2015). HDL-bound sphingosine-1-phosphate restrains lymphopoiesis and neuroinflammation. *Nature* 523, 342–346. [PubMed: 26053123]
5. Cartier A, and Hla T (2019). Sphingosine 1-phosphate: lipid signaling in pathology and therapy. *Science* 366, eaar5551. [PubMed: 31624181]
6. Deng X, Yin X, Allan R, Lu DD, Maurer CW, Haimovitz-Friedman A, Fuks Z, Shaham S, and Kolesnick R (2008). Ceramide biogenesis is required for radiation-induced apoptosis in the germ line of *C. elegans*. *Science* 322, 110–115. [PubMed: 18832646]
7. Futerman AH, and Hannun YA (2004). The complex life of simple sphingolipids. *EMBO Rep.* 5, 777–782. [PubMed: 15289826]
8. Hannun YA, and Obeid LM (2008). Principles of bioactive lipid signalling: lessons from sphingolipids. *Nat. Rev. Mol. Cell Biol* 9, 139–150. [PubMed: 18216770]
9. Hanson MA, Roth CB, Jo E, Griffith MT, Scott FL, Reinhart G, Desale H, Clemons B, Cahalan SM, Schuerer SC, et al. (2012). Crystal structure of a lipid G protein–coupled receptor. *Science* 335, 851–855. [PubMed: 22344443]
10. Janneh AH, and Ogretmen B (2022). Targeting sphingolipid metabolism as a therapeutic strategy in cancer treatment. *Cancers* 14, 2183. [PubMed: 35565311]
11. Liang J, Nagahashi M, Kim EY, Harikumar KB, Yamada A, Huang W-C, Hait NC, Allegood JC, Price MM, Avni D, et al. (2013). Sphingosine-1-phosphate links persistent STAT3 activation, chronic intestinal inflammation, and development of colitis-associated cancer. *Cancer Cell* 23, 107–120. [PubMed: 23273921]

12. Milstien S, and Spiegel S (2006). Targeting sphingosine-1-phosphate: a novel avenue for cancer therapeutics. *Cancer Cell* 9, 148–150. [PubMed: 16530698]
13. Ogretmen B, and Hannun YA (2004). Biologically active sphingolipids in cancer pathogenesis and treatment. *Nat. Rev. Cancer* 4, 604–616. [PubMed: 15286740]
14. Ponnusamy S, Selvam SP, Mehrotra S, Kawamori T, Snider AJ, Obeid LM, Shao Y, Sabbadini R, and Ogretmen B (2012). Communication between host organism and cancer cells is transduced by systemic sphingosine kinase 1/sphingosine 1-phosphate signalling to regulate tumour metastasis. *EMBO Mol. Med* 4, 761–775. [PubMed: 22707406]
15. Pyne NJ, and Pyne S (2010). Sphingosine 1-phosphate and cancer. *Nat. Rev. Cancer* 10, 489–503. [PubMed: 20555359]
16. Saddoughi SA, Gencer S, Peterson YK, Ward KE, Mukhopadhyay A, Oaks J, Bielawski J, Szulc ZM, Thomas RJ, Selvam SP, et al. (2013). Sphingosine analogue drug FTY720 targets I2PP2A/SET and mediates lung tumour suppression via activation of PP2A-RIPK1-dependent necroptosis. *EMBO Mol. Med* 5, 105–121. [PubMed: 23180565]
17. Menuz V, Howell KS, Gentina S, Epstein S, Riezman I, Fornallaz-Mulhauser M, Hengartner MO, Gomez M, Riezman H, and Martinou J-C (2009). Protection of *C. elegans* from anoxia by HYL-2 ceramide synthase. *Science* 324, 381–384. [PubMed: 19372430]
18. Obeid LM, Linaudic CM, Karolak LA, and Hannun YA (1993). Programmed cell death induced by ceramide. *Science* 259, 1769–1771. [PubMed: 8456305]
19. Johnson KR, Johnson KY, Crellin HG, Ogretmen B, Boylan AM, Harley RA, and Obeid LM (2005). Immunohistochemical distribution of sphingosine kinase 1 in normal and tumor lung tissue. *J. Histochem. Cytochem* 53, 1159–1166. [PubMed: 15923363]
20. Maceyka M, Payne SG, Milstien S, and Spiegel S (2002). Sphingosine kinase, sphingosine-1-phosphate, and apoptosis. *Biochim. Biophys. Acta* 1585, 193–201. [PubMed: 12531554]
21. Payne SG, Milstien S, and Spiegel S (2002). Sphingosine-1-phosphate: dual messenger functions. *FEBS Lett.* 531, 54–57. [PubMed: 12401202]
22. Kawamori T, Osta W, Johnson KR, Pettus BJ, Bielawski J, Tanaka T, Wargovich MJ, Reddy BS, Hannun YA, Obeid LM, and Zhou D (2006). Sphingosine kinase 1 is up-regulated in colon carcinogenesis. *Faseb. J.* 20, 386–388. [PubMed: 16319132]
23. Li J, Guan H-Y, Gong L-Y, Song L-B, Zhang N, Wu J, Yuan J, Zheng Y-J, Huang Z-S, and Li M (2008). Clinical significance of sphingosine kinase-1 expression in human astrocytomas progression and overall patient survival. *Clin. Cancer Res* 14, 6996–7003. [PubMed: 18980995]
24. Song L, Xiong H, Li J, Liao W, Wang L, Wu J, and Li M (2011). Sphingosine kinase-1 enhances resistance to apoptosis through activation of PI3K/Akt/NF- κ B pathway in human non-small cell lung cancer. *Clin. Cancer Res* 17, 1839–1849. [PubMed: 21325072]
25. Issuree PDA, Pushparaj PN, Pervaiz S, and Melendez AJ (2009). Resveratrol attenuates C5a-induced inflammatory responses in vitro and in vivo by inhibiting phospholipase D and sphingosine kinase activities. *FASEB J.* 23, 2412–2424. [PubMed: 19346296]
26. Ratajczak MZ, Kim C, Wu W, Shin DM, Bryndza E, Kucia M, and Ratajczak J (2012). The role of innate immunity in trafficking of hematopoietic stem cells—an emerging link between activation of complement cascade and chemotactic gradients of bioactive sphingolipids. *Adv. Exp. Med. Biol* 946, 37–54. [PubMed: 21948361]
27. Kim CH, Wu W, Wysoczynski M, Abdel-Latif A, Sunkara M, Morris A, Kucia M, Ratajczak J, and Ratajczak MZ (2012). Conditioning for hematopoietic transplantation activates the complement cascade and induces a proteolytic environment in bone marrow: a novel role for bioactive lipids and soluble C5b-C9 as homing factors. *Leukemia* 26, 106–116. [PubMed: 21769103]
28. Herbert A (2020). Complement controls the immune synapse and tumors control complement. *J. Immunother. Cancer* 8, e001712. [PubMed: 33323465]
29. Roumenina LT, Daugan MV, Petitprez F, Sautès-Fridman C, and Fridman WH (2019). Context-dependent roles of complement in cancer. *Nat. Rev. Cancer* 19, 698–715. [PubMed: 31666715]
30. Hla T, Venkataraman K, and Michaud J (2008). The vascular S1P gradient—cellular sources and biological significance. *Biochim. Biophys. Acta* 1781, 477–482. [PubMed: 18674637]

31. Bachmaier K, Guzman E, Kawamura T, Gao X, and Malik AB (2012). Sphingosine kinase 1 mediation of expression of the anaphylatoxin receptor C5L2 dampens the inflammatory response to endotoxin. *PLoS One* 7, e30742. [PubMed: 22355325]
32. Chi H (2011). Sphingosine-1-phosphate and immune regulation: trafficking and beyond. *Trends Pharmacol. Sci* 32, 16–24. [PubMed: 21159389]
33. Halova I, Draberova L, and Draber P (2012). Mast cell chemotaxis–chemoattractants and signaling pathways. *Front. Immunol* 3, 119. [PubMed: 22654878]
34. Ratajczak MZ, Borkowska S, and Ratajczak J (2013). An emerging link in stem cell mobilization between activation of the complement cascade and the chemotactic gradient of sphingosine-1-phosphate. *Prostaglandins Other Lipid Mediat.* 104–105, 122–129. [PubMed: 22981511]
35. Jeon S, Song J, Lee D, Kim G-T, Park S-H, Shin D-Y, Shin K-O, Park K, Shim S-M, and Park T-S (2020). Inhibition of sphingosine 1-phosphate lyase activates human keratinocyte differentiation and attenuates psoriasis in mice. *J. Lipid Res* 61, 20–32. [PubMed: 31690639]
36. Neun BW, Ilinskaya AN, and Dobrovolskaia MA (2018). Analysis of complement activation by nanoparticles. In *Characterization of Nanoparticles Intended for Drug Delivery* (Springer), pp. 149–160.
37. Chakraborty P, Vaena SG, Thyagarajan K, Chatterjee S, Al-Khami A, Selvam SP, Nguyen H, Kang I, Wyatt MW, Baliga U, et al. (2019). Pro-survival lipid sphingosine-1-phosphate metabolically programs T cells to limit anti-tumor activity. *Cell Rep.* 28, 1879–1893.e7. [PubMed: 31412253]
38. Janneh AH, Kassir MF, Dwyer CJ, Chakraborty P, Pierce JS, Flume PA, Li H, Nadig SN, Mehrotra S, and Ogretmen B (2021). Alterations of lipid metabolism provide serologic biomarkers for the detection of asymptomatic versus symptomatic COVID-19 patients. *Sci. Rep* 11, 14232. [PubMed: 34244584]
39. Teijaro JR, Studer S, Leaf N, Kiosses WB, Nguyen N, Matsuki K, Negishi H, Taniguchi T, Oldstone MBA, and Rosen H (2016). S1PR1-mediated IFNAR1 degradation modulates plasmacytoid dendritic cell interferon- α autoamplification. *Proc. Natl. Acad. Sci. USA* 113, 1351–1356. [PubMed: 26787880]
40. Wilkerson BA, Grass GD, Wing SB, Argraves WS, and Argraves KM (2012). Sphingosine 1-phosphate (S1P) carrier-dependent regulation of endothelial barrier: high density lipoprotein (HDL)-S1P prolongs endothelial barrier enhancement as compared with albumin-S1P via effects on levels, trafficking, and signaling of S1P1. *J. Biol. Chem* 287, 44645–44653. [PubMed: 23135269]
41. Mann SS, Pettenati MJ, von Kap-herr C, and Hart TC (1998). Reassignment of peptidyl prolyl isomerase-like 1 gene (PPIL1) to human chromosome region 6p21. 1 by radiation hybrid mapping and fluorescence in situ hybridization. *Cytogenet. Cell Genet* 83, 228–229. [PubMed: 10072585]
42. Obama K, Kato T, Hasegawa S, Satoh S, Nakamura Y, and Furukawa Y (2006). Overexpression of peptidyl-prolyl isomerase-like 1 is associated with the growth of colon cancer cells. *Clin. Cancer Res* 12, 70–76. [PubMed: 16397026]
43. Minn AJ, Gupta GP, Siegel PM, Bos PD, Shu W, Giri DD, Viale A, Olshen AB, Gerald WL, and Massagué J (2005). Genes that mediate breast cancer metastasis to lung. *Nature* 436, 518–524. [PubMed: 16049480]
44. Liszewski MK, Kolev M, Le Friec G, Leung M, Bertram PG, Fara AF, Subias M, Pickering MC, Drouet C, Meri S, et al. (2013). Intracellular complement activation sustains T cell homeostasis and mediates effector differentiation. *Immunity* 39, 1143–1157. [PubMed: 24315997]
45. Oleinik N, Kim J, Roth BM, Selvam SP, Gooz M, Johnson RH, Lemasters JJ, and Ogretmen B (2019). Mitochondrial protein import is regulated by p17/PERMIT to mediate lipid metabolism and cellular stress. *Sci. Adv* 5, eaax1978. [PubMed: 31535025]
46. Montaudon E, Nikitorowicz-Buniak J, Sourd L, Morisset L, El Botty R, Huguet L, Dahmani A, Painsec P, Némati F, Vacher S, et al. (2020). PLK1 inhibition exhibits strong anti-tumoral activity in CCND1-driven breast cancer metastases with acquired palbociclib resistance. *Nat. Commun* 11, 4053. [PubMed: 32792481]
47. Jager MJ, Shields CL, Cebulla CM, Abdel-Rahman MH, Grossniklaus HE, Stern M-H, Carvajal RD, Belfort RN, Jia R, Shields JA, and Damato BE (2020). Uveal melanoma. *Nat. Rev. Dis. Primers* 6, 24–25. [PubMed: 32273508]

48. Atkinson C, He S, Morris K, Qiao F, Casey S, Goddard M, and Tomlinson S (2010). Targeted complement inhibitors protect against posttransplant cardiac ischemia and reperfusion injury and reveal an important role for the alternative pathway of complement activation. *J. Immunol* 185, 7007–7013. [PubMed: 20962256]
49. Atkinson C, Varela JC, and Tomlinson S (2009). Complement-dependent inflammation and injury in a murine model of brain dead donor hearts. *Circ. Res* 105, 1094–1101. [PubMed: 19815824]
50. Liu L, Li W, Li Z, and Kirschfink M (2012). Sublytic complement protects prostate cancer cells from tumour necrosis factor- α -induced cell death. *Clin. Exp. Immunol* 169, 100–108. [PubMed: 22774984]
51. Elvington M, Huang Y, Morgan BP, Qiao F, Van Rooijen N, Atkinson C, and Tomlinson S (2012). A targeted complement-dependent strategy to improve the outcome of mAb therapy, and characterization in a murine model of metastatic cancer. *Blood* 119, 6043–6051. [PubMed: 22442351]
52. Langer HF, Chung K-J, Orlova VV, Choi EY, Kaul S, Kruhlak MJ, Alatsianos M, DeAngelis RA, Roche PA, Magotti P, et al. (2010). Complement-mediated inhibition of neovascularization reveals a point of convergence between innate immunity and angiogenesis. *Blood* 116, 4395–4403. [PubMed: 20625009]
53. Nunez-Cruz S, Gimotty PA, Guerra MW, Connolly DC, Wu Y-Q, DeAngelis RA, Lambris JD, Coukos G, and Scholler N (2012). Genetic and pharmacologic inhibition of complement impairs endothelial cell function and ablates ovarian cancer neovascularization. *Neoplasia* 14, 994–1004. [PubMed: 23226093]
54. Chen J, Sun Z.-h., Chen L.-y., Xu F, Zhao Y.-p., Li G.-q., Tang M, Li Y, Zheng Q.-y., Wang S.-f., et al. (2020). C5aR deficiency attenuates the breast cancer development via the p38/p21 axis. *Aging (Albany NY)* 12, 14285–14299. [PubMed: 32669478]
55. Fuenmayor J, Perez-Vazquez K, Perez-Witzke D, Penichet ML, and Montano RF (2010). Decreased survival of human breast cancer cells expressing HER2/neu on in vitro incubation with an anti-HER2/neu antibody fused to C5a or C5adesArg. *Mol. Cancer Ther* 9, 2175–2185. [PubMed: 20682652]
56. Imamura T, Yamamoto-Ibusuki M, Sueta A, Kubo T, Irie A, Kikuchi K, Kariu T, and Iwase H (2016). Influence of the C5a–C5a receptor system on breast cancer progression and patient prognosis. *Breast Cancer* 23, 876–885. [PubMed: 26494574]
57. Jackson WD, Gulino A, Fossati-Jimack L, Castro Seoane R, Tian K, Best K, Köhl J, Belmonte B, Strid J, and Botto M (2021). C3 drives inflammatory skin carcinogenesis independently of C5. *J. Invest. Dermatol* 141, 404–414.e6. [PubMed: 32682912]
58. Kwak JW, Laskowski J, Li HY, McSharry MV, Sippel TR, Bullock BL, Johnson AM, Poczobutt JM, Neuwelt AJ, Malkoski SP, et al. (2018). Complement activation via a C3a receptor pathway alters CD4⁺ T lymphocytes and mediates lung cancer progression. *Cancer Res.* 78, 143–156. [PubMed: 29118090]
59. Zhang Q, Han M, Wang W, Song Y, Chen G, Wang Z, and Liang Z (2015). Downregulation of cathepsin L suppresses cancer invasion and migration by inhibiting transforming growth factor- β -mediated epithelial-mesenchymal transition. *Oncol. Rep* 33, 1851–1859. [PubMed: 25632968]
60. Fei Y, Xiong Y, Shen X, Zhao Y, Zhu Y, Wang L, and Liang Z (2018). Cathepsin L promotes ionizing radiation-induced U251 glioma cell migration and invasion through regulating the GSK-3 β /CUX1 pathway. *Cell. Signal* 44, 62–71. [PubMed: 29331585]
61. Pranjol MZI, Zinovkin DA, Maskell ART, Stephens LJ, Achinovich SL, Los DM, Nadyrov EA, Hannemann M, Gutowski NJ, and Whatmore JL (2019). Cathepsin L-induced galectin-1 may act as a proangiogenic factor in the metastasis of high-grade serous carcinoma. *J. Transl. Med* 17, 216. [PubMed: 31269957]
62. Chai G, Webb A, Li C, Antaki D, Lee S, Breuss MW, Lang N, Stanley V, Anzenberg P, Yang X, et al. (2021). Mutations in spliceosomal genes PPIL1 and PRP17 cause neurodegenerative pontocerebellar hypoplasia with microcephaly. *Neuron* 109, 241–256.e9. [PubMed: 33220177]
63. Stegmann CM, Lührmann R, and Wahl MC (2010). The crystal structure of PPIL1 bound to cyclosporine A suggests a binding mode for a linear epitope of the SKIP protein. *PLoS One* 5, e10013. [PubMed: 20368803]

64. Asgari E, Le Fric G, Yamamoto H, Perucha E, Sacks SS, Köhl J, Cook HT, and Kemper C (2013). C3a modulates IL-1 β secretion in human monocytes by regulating ATP efflux and subsequent NLRP3 inflammasome activation. *Blood* 122, 3473–3481. [PubMed: 23878142]
65. Arbore G, West EE, Spolski R, Robertson AAB, Klos A, Rheinheimer C, Dutow P, Woodruff TM, Yu ZX, O’Neill LA, et al. (2016). T helper 1 immunity requires complement-driven NLRP3 inflammasome activity in CD4+ T cells. *Science* 352, aad1210. [PubMed: 27313051]
66. Comeau SR, Gatchell DW, Vajda S, and Camacho CJ (2004). ClusPro: an automated docking and discrimination method for the prediction of protein complexes. *Bioinformatics* 20, 45–50. [PubMed: 14693807]

Highlights

- Increased S1P metabolism activates C3 complement processing through S1PR1
- S1P/S1PR1-activated intracellular C3b- α'_2 associates with PPIL1 inducing inflammasome
- The S1PR1/C3/PPIL1/NLRP3 axis mediates cancer cell migration and tumor metastasis
- Targeting S1PR1/C3/NLRP3 signaling prevents lung colonization/metastasis

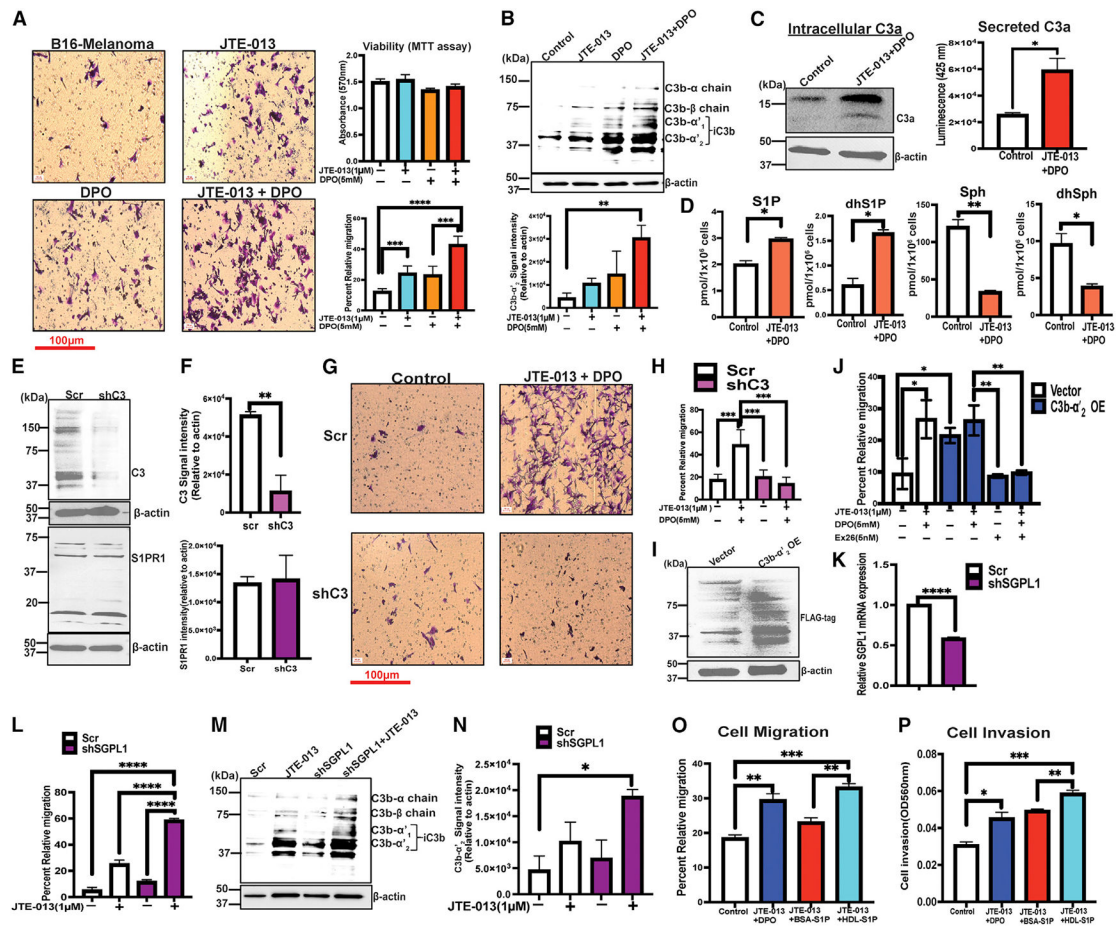


Figure 1. JTE-013 and DPO drug combination increases B16 cell migration in response to elevated intracellular S1P/S1PR1/C3 signaling

(A) Migration of B16 cells in the absence/presence of JTE-013 (1 μ M) for 24 h, DPO (5 mM) for 8 h, or JTE + DPO combination for 24 h (JTE-013 pre-treatment alone for 16 h and then with DPO addition for 8 h), was measured in Boyden chambers. Representative images of migrated cells (left panels), and optical density readings of transwell inserts at 630 nm, after staining with crystal violet solution (0.5%) (lower left graph) are shown. In similar studies, the effects of these treatments on B16 cell viability were measured by MTT cell proliferation assay (upper left graph). Scale bars, 100 μ m.

(B) Effects of JTE-013/DPO (alone or in combination) on complement C3b- α and - β chain expression were measured in B16 cells using western blotting (upper panel). Actin was used as a loading control. Western blotting was quantified relative to actin levels (lower graph).

(C) Effects of JTE/DPO (alone or in combination) on intracellular C3a expression and secretion in B16 cells were measured by western blotting (left panel) and ELISA (right panel), respectively, using anti-C3a-antibody.

(D) Intracellular levels of S1P, dhS1P, Sph, and dhSph in B16 cells treated with vehicle or JTE-013/DPO combination were measured by lipidomics as we described.^{37,38}

(E–H) Migration of B16 cells transfected with shRNA scrambled (Scr) or shRNA C3 knockdown (shC3) plasmids, confirmed by western blotting and quantified, without

significantly affecting S1PR1 expression (E and F) was measured in Boyden chambers in response to JTE013/DPO treatment (G and H). Scale bars, 100 μm .

(I and J) Migration of B16 cells transfected for ectopic expression of wild-type (WT)-C3b- α'_{2} (vector-only transfected cells were used as controls), confirmed by western blotting (I) was measured in Boyden chambers with/without JTE-013/DPO exposure (J).

(K–N) Effects of shRNA-mediated knockdown of S1P lyase (shS1PL1) compared with shRNA scrambled (Scr) transfected B16 cells, confirmed using qRT-PCR (K), on cell migration (L) or C3b expression (M and N) were measured using Boyden chambers and western blotting, respectively.

(O and P) Effects of exogenous S1P with BSA- or HDL-S1P + JTE-013 combination, compared with endogenous S1P with DPO + JTE-013 combination on migration (O) and invasion (P) assays using B16 cells. Data represent at least two independent studies in triplicates. Data are means of \pm SD. * $p < 0.05$, ** $p < 0.01$, *** $p < 0.001$, **** $p < 0.0001$.

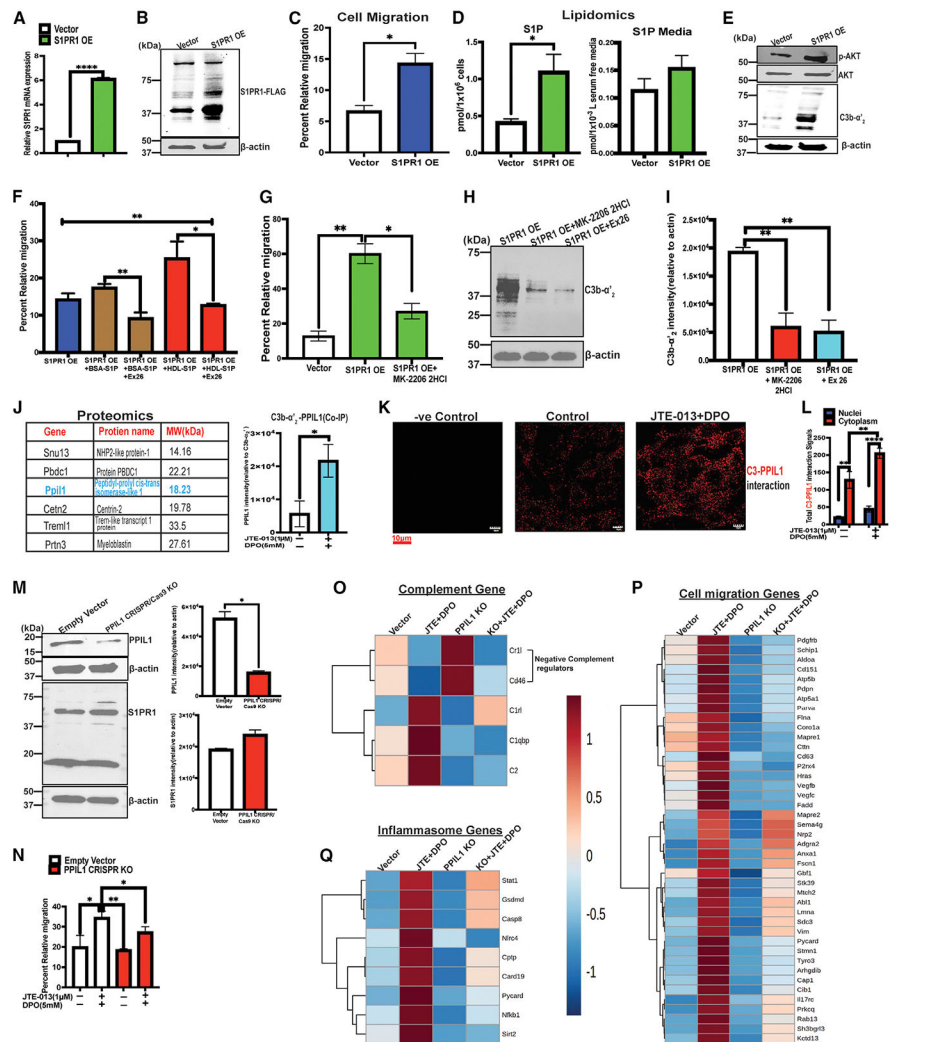


Figure 2. S1P/S1PR1 signaling induces the C3-PPIL1 interaction complex

(A and B) S1PR1 overexpression (S1PR1 OE) with FLAG tag plasmid was expressed in B16 cells (with vector-transfected cells as control) and was confirmed with qRT-PCR, indicating S1PR1 mRNA levels (A) and western blot detecting S1PR1 FLAG tag (B). (C) Cell migration effects of S1PR1 OE cells (vector as control). (D) Intracellular and extracellular levels of S1P in S1PR1 OE cells (vector as control). (E) The effects on p-AKT, total AKT, and C3b- α' ₂ protein expressions were analyzed by western blotting. (F) Cell migration effects on S1PR1 OE cells in the absence/presence of Ex26, BSA-S1P (0.5 μ M), and HDL-S1P (0.5 μ M) for 24 h were measured in Boyden chambers. (G) Cell migration effects of AKT inhibitor (MK-2206 2HCL) on S1PR1 OE B16 cells and vector as controls were measured in Boyden chambers. (H and I) Effects of MK-2206 2HCL and Ex26 on C3b- α' ₂ protein expression in S1PR1 OE B16 cells were analyzed with western blotting (H) and quantified (I). (J–L) B16 cells were treated with JTE-013 + DPO for 24 h (with the vehicle as control). Cells were lysed, and C3 was co-immunoprecipitated (co-IP) using an anti-C3 antibody

followed by proteomics (an anti-IgG antibody was used as a negative control). Six proteins whose association with C3 was enhanced in response to JTE-013 + DPO treatment were identified (J) (left panel), and only C3-PPIL1 association was verified by co-IP (J) (right panel) and by proximity ligation assay (K and L). Scale bars, 10 μ m.

(M and N) CRISPR-Cas9-mediated PPIL1 knockout (KO) compared with empty vector control was confirmed by western blotting without significantly affecting S1PR1 expression (M) (left panel) and quantified (M) (right panel). In addition, the effects of PPIL1 KO on cell migration in the absence/presence of JTE-013 + DPO for 24 h were measured in Boyden chambers (N).

(O–Q) Heatmaps of RNA-seq analyses on the effects of PPIL1 KO in B16 cells in response to JTE-013 + DPO treatment, compared with vector controls, to depict the up- and downregulations of gene. Genes that are involved in the regulation of complement signaling (O), cell migration (P), and inflammasome formation (Q) were analyzed. Three independent experimental samples per group were combined to produce a single RNA sample per group that was sent to Novogene for RNA-seq. Data represent at least two independent studies in triplicates. Data are means of \pm SD. * $p < 0.05$, ** $p < 0.01$, *** $p < 0.001$, **** $p < 0.0001$.

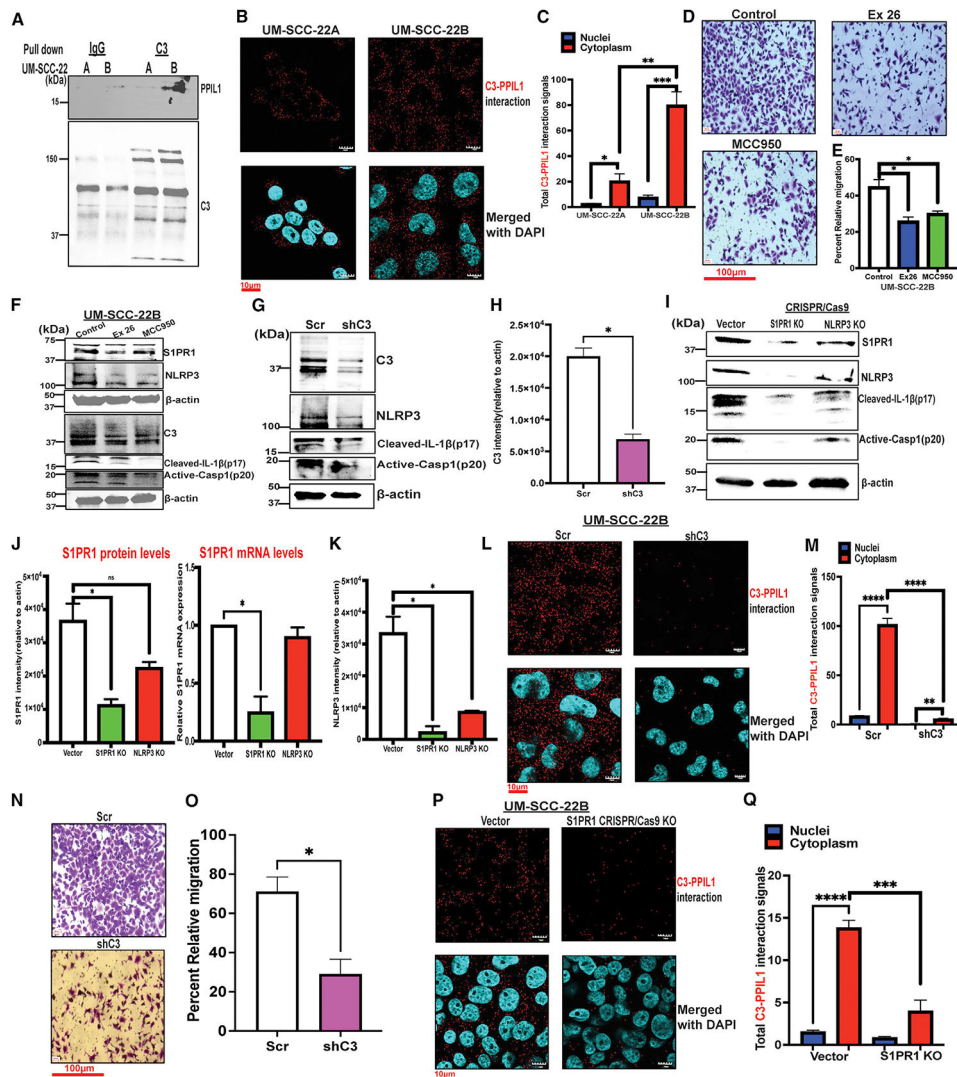


Figure 3. Metastatic UM-SCC-22B cell line exhibits enhanced C3-PPIL1 association complex to regulate NLRP3 inflammasome signaling
 (A–C) UM-SCC-22A primary versus UM-SCC-22B metastatic human head and neck cancer cell lines were analyzed. C3-PPIL1 binding complex in metastatic UM-SCC-22B compared with UM-SCC-22A was determined by pulling down C3 with anti-C3 antibody (anti-IgG as negative control), followed by western blot detection of PPIL1 (A). Proximity ligation assay consistently showed an enhanced C3-PPIL1 binding in UM-SCC-22B compared with UM-SCC-22A cell lines (B and C). Scale bars, 10 μ m.
 (D–F) Effects of Ex26 (5 nM) and MCC950 (10 μ M) on UM-SCC-22B cell line for 24 h. Representative images of UM-SCC-22B migrated cells after treatments, including vehicle-treated controls, as observed in Boyden chambers (D) and optical density readings of trans well inserts at 630 nm after staining with crystal violet solution (0.5%) (E). In addition, the treatment effects on the expressions of S1PR1, C3, and NLRP3 inflammasome genes were further analyzed by western blotting (F). Scale bars, 100 μ m.
 (G–K) Effects of C3 shRNA knockdown (shC3), CRISPR-Cas9-mediated S1PR1 and NLRP3 knockout (KO) in UM-SCC-22B cell lines. Confirmation of C3 knockdown, and

its effects on downstream NLRP3, IL-1 β , and caspase-1, were analyzed by western blotting, compared with shRNA scrambled (Scr) (G). The C3 expression was quantified relative to actin (H). Confirmation of CRISPR-Cas9-mediated S1PR1 KO and NLRP3 KO and their effects on downstream genes were analyzed by western blotting compared with empty vector control (I). S1PR1 protein expressions were quantified (J) (left panel), and S1PR1 relative mRNA levels were analyzed with qRT-PCR (J) (right panel). NLRP3 protein expressions were quantified (K).

(L and M) Effects of UM-SCC-22B cells expressing shC3. C3-PPIL1 binding complex was analyzed by proximity ligation assay compared with SCR. Scale bars, 10 μ m. (N and O) Cell migration effects on UM-SCC-22B cells expressing shC3 (compared with Scr) were measured in Boyden chambers. Representative images of migrated cells (N), and optical density readings of transwell inserts at 630 nm, after staining with crystal violet solution (0.5%) (O). Scale bars, 100 μ m.

(P and Q) C3-PPIL1 binding effects in UM-SCC-22B cells expressing CRISPR-Cas9-mediated S1PR1 KO (compared with vector) were analyzed by proximity ligation assay. Scale bars, 10 μ m. Data represent at least two independent studies in triplicates. Data are means of \pm SD. * $p < 0.05$, ** $p < 0.01$, *** $p < 0.001$, **** $p < 0.0001$.

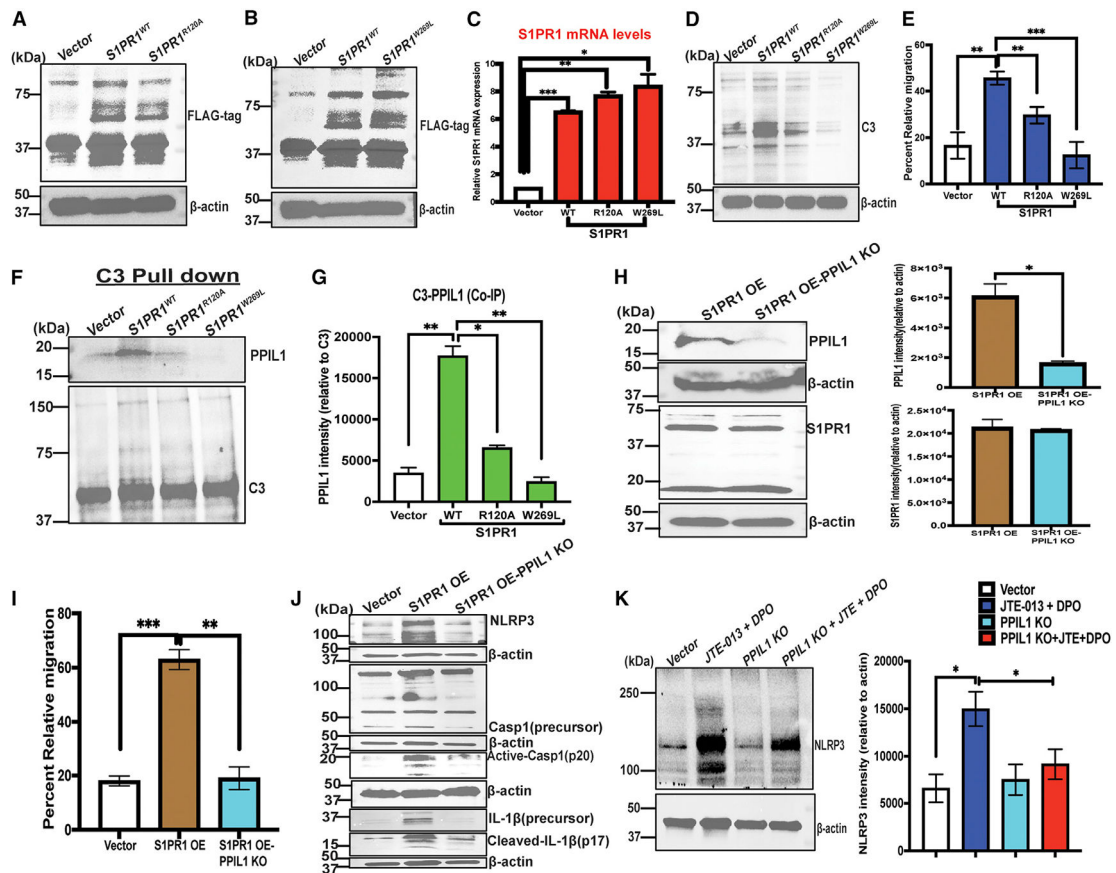


Figure 4. S1PR1 regulates the C3-PPIL1 binding complex and inflammasome activation to induce cell migration

(A–C) S1PR1 mutants, arginine 120 to alanine (R120A), and tryptophan 269 to leucine (W269L) were expressed with FLAG tag in B16 cell line and analyzed by western blotting, compared with wild-type (WT) S1PR1 and vector controls (A and B). In contrast, their relative S1PR1 mRNA levels were analyzed by qRT-PCR (C). (D and E) The effects of S1PR1 mutants on C3 protein expression and cell migration in comparison with WT-S1PR1 or vector control were analyzed by western blotting (D) and Boyden chambers (E), respectively.

(F and G) S1PR1 mutants and WT-S1PR1 (precursor) or vector B16 cells were lysed, and C3 was pulled down or subjected to co-IP to determine the effects of C3-PPIL1 association in the mutants' cells. To detect PPIL1 binding in the C3 pull-down lysates, western blotting was performed (F) and quantified (G).

(H–J) CRISPR-Cas9-mediated PPIL1 knockout (PPIL1 KO) in S1PR1 overexpression (S1PR1 OE) B16 cells was analyzed by western blotting and quantified, using S1PR1 OE as control, without affecting S1PR1 expression (H). In addition, the Effects of PPIL1 KO in S1PR1 OE cells on cell migration and NLRP3 inflammasome genes compared with vector or S1PR1 OE controls were measured in Boyden chambers (I) and analyzed by western blotting (J), respectively.

(K) Effects of PPIL1 KO in response to JTE-013 + DPO treatment for 24 h on NLRP3 protein expression were analyzed by western blotting and quantified, compared with vector

or JTE-013 + DPO controls. Data represent at least two independent studies in triplicates. Data are means of \pm SD. * $p < 0.05$, ** $p < 0.01$, *** $p < 0.001$, **** $p < 0.0001$.

Author Manuscript

Author Manuscript

Author Manuscript

Author Manuscript

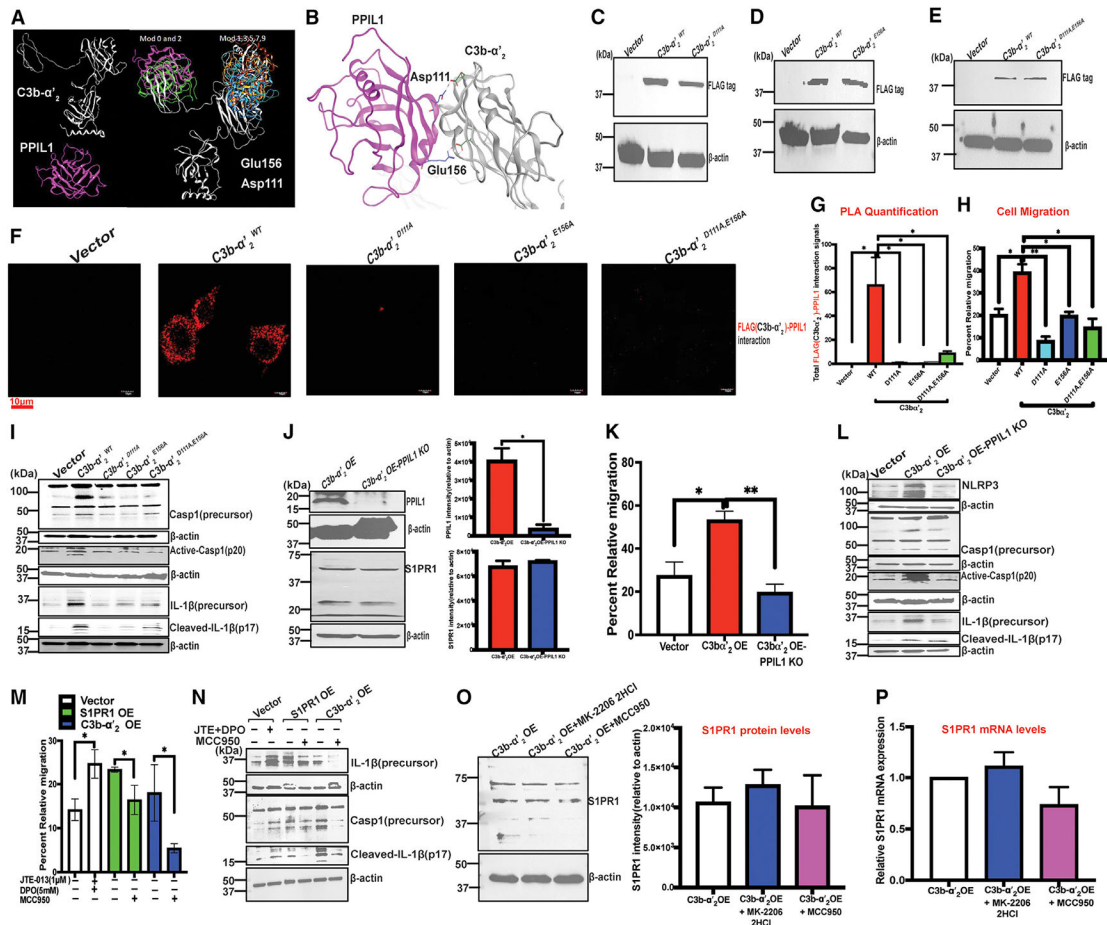


Figure 5. Mutant C3b-α'2 prevents C3b-α'2-PPIL1 binding, inflammasome activation, and cell migration

(A–E) Bimolecular docking simulations based on X-ray structural information identified several residues that are vital for the C3-PPIL1 binding complex, including glutamic acid 156 (E156) and aspartic acid 111 (D111), as critical residues involved in C3b-α'2-PPIL1 interaction (A and B). Mutants D111A (C), E156A (D), and double mutants, 2X (E) with comparison with wild-type (WT) C3b-α'2 overexpression and empty vector controls were expressed with FLAG tag in B16 cell line and analyzed by western blotting. (F–G) Binding interaction effects of the three C3b-α'2 mutants' (D111A, E156A, 2X) with PPIL1 as detected by proximity ligation assay (PLA), compared with WT-C3b-α'2 and empty vector controls (F). This binding interaction is quantified in (G). Scale bars, 10 μm. (H and I) Effects of C3b-α'2 mutants on cell migration and inflammasome genes, compared with WT-C3b-α'2 and empty vector controls, were measured in Boyden chambers (H) and analyzed by western blotting (I), respectively. (J–L) CRISPR-Cas9-mediated PPIL1 knockout (PPIL1 KO) in C3b-α'2 overexpression (C3b-α'2 OE) B16 cells was confirmed by western blot and quantified, as compared with C3b-α'2 OE control, without affecting S1PR1 protein expression levels (J). The PPIL1 KO effects on cell migration and NLRP3 inflammasome genes were measured with Boyden chambers (K) and analyzed by western blotting (L), respectively, compared with vector and C3b-α'2 OE controls.

(M) Migration of vector, S1PR1 overexpression (S1PR1 OE), C3b- α' ₂ OE B16 cells in the absence/presence of JTE + DPO combination for 24 h (JTE-013 pre-treatment alone for 16 h and then with DPO addition for 8 h) and MCC950 for 24 h, was measured in Boyden chambers.

(N) Effects of vector, S1PR1 OE, and C3b- α' ₂ OE cells on NLRP3 inflammasome genes in the absence/presence of JTE + DPO combination and MCC950 were analyzed by western blotting.

(O and P) S1PR1 protein expression effects with absence/presence of AKT inhibitor (MK-2206 2HCl) and NLRP3 inhibitor (MCC950) on C3b- α' ₂ OE cells were analyzed by western blotting (O) (left panel) and quantified (O) (right panel). S1PR1 relative mRNA levels were analyzed by qRT-PCR (P). Data represent at least two independent studies in triplicates. Data are means of \pm SD. * $p < 0.05$, ** $p < 0.01$, *** $p < 0.001$, **** $p < 0.0001$.

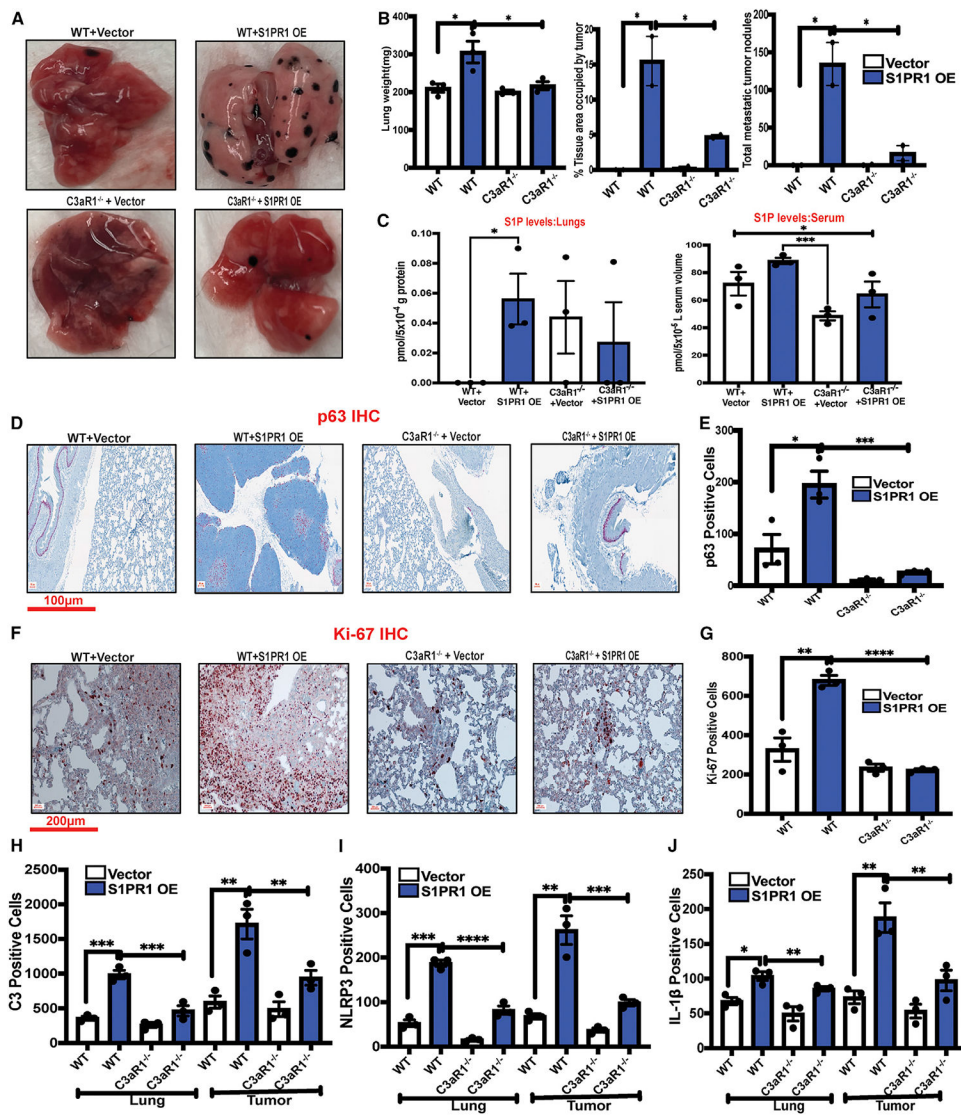


Figure 6. C3aR1^{-/-} knockout mice prevent lung metastasis induced by S1PR1 overexpression B16 cells

(A and B) B16 cells (25×10^4) expressing S1PR1 overexpression (S1PR1 OE) plasmid, or vector, were injected via tail vein of C3aR1^{-/-} knockout mice or C57BL/6J wild-type (WT) mice. All mice were sacrificed on day 21, and the representative images show tumor nodules of lung colonization/metastasis (A). The bar graphs represent lung weight (n = 3), percent tissue area occupied by tumors (n = 2), and total metastatic tumor nodules (n = 2) (B).

(C) S1P levels in the lung tissues (left panel) and serum (right panel) of C3aR1^{-/-} and C57BL/6J mice injected with either vector or S1PR1 OE cells. n = 3.

(D and E) Representative images with quantification showing immunohistochemistry of p63 melanoma marker in the lung tissues of C3aR1^{-/-} and C57BL/6J mice injected with either vector or S1PR1 OE cells. n = 3. Scale bars, 100 μ m.

(F and G) Representative images with quantification showing immunohistochemistry of Ki-67 metastatic marker in the lung tissues of C3aR1^{-/-} and C57BL/6J mice injected with either vector or S1PR1 OE cells. n = 3. Scale bars, 200 μ m.

(H–J) RNA scope *in situ* hybridization in lung tissues of C3aR1^{-/-}, and C57BL/6J mice injected with either vector or S1PR1 OE cells. The RNA scope analyses of C3 (H), NLRP3 (I), and IL-1 β (J) RNA expressions indicated by positive cells. n = 3. Scale bars, 100 μ m. Data are means of \pm SEM. *p < 0.05, **p < 0.01, ***p < 0.001, ****p < 0.0001.

Author Manuscript

Author Manuscript

Author Manuscript

Author Manuscript

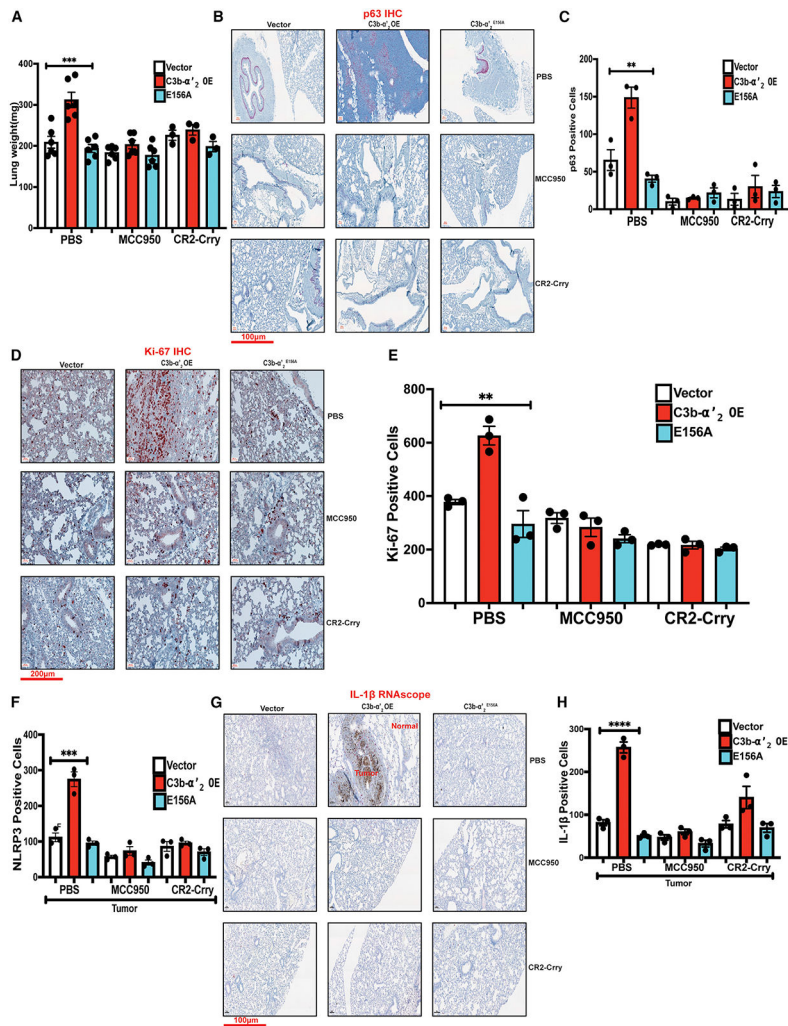


Figure 7. CR2-Crry (C3 inhibitor) and MCC950 (NLRP3 inhibitor) pharmacological compounds attenuate S1P/S1PR1/C3/inflammasome-mediated tumor metastasis *in vivo*

(A) B16 cells (25×10^4) expressing C3b- $\alpha'2$ overexpression (C3b- $\alpha'2$ OE) plasmid, C3b- $\alpha'2$ E156A mutant, or vector were injected via tail vein of C57BL/6J mice and treated intraperitoneally (i.p.) with 20 mg/kg MCC950 (n = 6), 10 mg/kg CR2-Crry (n = 3), or PBS (n = 6). All mice were sacrificed on day 21, and the bar graph represents lung weight.

(B and C) Representative images with quantification showing immunohistochemistry of p63 melanoma marker in the lung tissues of C57BL/6J mice injected with C3b- $\alpha'2$ OE, C3b- $\alpha'2$ E156A mutant, or vector B16 cells and treated i.p. with MCC950 (n = 3), CR2-Crry (n = 3), or PBS (n = 3). Scale bars, 100 μ m.

(D and E) Representative images with quantification showing immunohistochemistry of Ki-67 metastatic marker in the lung tissues of C57BL/6J mice injected with C3b- $\alpha'2$ OE, C3b- $\alpha'2$ E156A mutant, or vector B16 cells and treated i.p. with MCC950 (n = 3), CR2-Crry (n = 3), or PBS (n = 3). Scale bars, 200 μ m.

(F-H) RNA scope *in situ* hybridization in lung tissues of C57BL/6J mice injected with C3b- $\alpha'2$ OE, C3b- $\alpha'2$ E156A mutant, or vector B16 cells and treated i.p. with MCC950 (n = 3), CR2-Crry (n = 3), or PBS (n = 3). The RNA scope analyses of NLRP3 RNA

expressions indicated by positive cells (F). Representative images and quantification of IL-1 β expressions (G and H). Scale bars, 100 μ m. Data are means of \pm SD. * $p < 0.05$, ** $p < 0.01$, *** $p < 0.001$, **** $p < 0.0001$.

Author Manuscript

Author Manuscript

Author Manuscript

Author Manuscript

KEY RESOURCES TABLE

REAGENT or RESOURCE	SOURCE	IDENTIFIER
Antibodies		
Anti-mouse complement C3 goat IgG fraction, peroxidase-conjugated	MP Biomedicals, LLC	Cat# 0855557, RRID:AB_2334545
C3 Antibody (B-9)	Santa Cruz Biotechnology	Cat# Cat# sc-28294, RRID:AB_627277
Recombinant Anti-C3 antibody [EPR19394]	Abcam	Cat# ab200999
S1PR1/EDG1 antibody	Proteintech	Cat# 55133-1-AP, RRID:AB_10793721
Anti-Sphingosine 1-phosphate receptor 1 (S1PR1) Antibody	MilliporeSigma	Cat# MABC94, RRID:AB_2665518
Human S1P1/EDG-1 APC-conjugated Antibody	R&D systems	Cat# FAB2016A, RRID:AB_2184740
Mouse S1P1/EDG-1 PE-conjugated Antibody	R&D systems	Cat# FAB7089P, RRID:AB_10994187
S1P2/EDG-5/S1PR2 Antibody	Novus Biologicals	Cat# NBP2-26691
S1PR2 Polyclonal antibody	ProteinTech	Cat# 21180-1-AP, RRID:AB_10694573
PP1L1 Antibody (LB-72)	Santa Cruz Biotechnology	Cat# sc-100701, RRID:AB_2169604
anti-PP1L1 antibody	MyBiosource	Cat# MBS9416271
caspase-1 Antibody (14F468)	Santa Cruz Biotechnology	Cat# sc-56036, RRID:AB_781816
normal mouse IgG	Santa Cruz Biotechnology	Cat# sc-2025, RRID:AB_737182
Normal Rabbit IgG	Cell Signaling Technology	Cat# 2729, RRID:AB_1031062
Anti-rat IgG, HRP-linked Antibody	Cell Signaling Technology	Cat# 7077, RRID:AB_10694715
Anti-rabbit IgG, HRP-linked Antibody	Cell Signaling Technology	Cat# 7074, RRID:AB_2099233
Anti-mouse IgG, HRP-linked Antibody	Cell Signaling Technology	Cat# 7076, RRID:AB_330924
β -Actin (13E5) Rabbit mAb	Cell Signaling Technology	Cat# 4970, RRID:AB_2223172
Phospho-Akt (Ser473) Antibody	Cell Signaling Technology	Cat# 9271, RRID:AB_329825
Akt Antibody	Cell Signaling Technology	Cat# 9272, RRID:AB_329827
DYKDDDDK Tag Antibody	Cell Signaling Technology	Cat# 2368, RRID:AB_2217020
IL-1 β (3A6) Mouse mAb	Cell Signaling Technology	Cat# 12242, RRID:AB_2715503
Human/Mouse NLRP3/NALP3 Antibody	R&D systems	Cat# MAB7578, RRID:AB_2889405
Ki-67 (D3B5) Rabbit mAb (Mouse Preferred; IHC Formulated)	Cell Signaling Technology	Cat# 12202, RRID:AB_2620142
Rabbit TrueBlot [®] : Anti-Rabbit IgG HRP	Rockland Immunochemical, Inc.	Cat# 18-8816-33, RRID:AB_2610848
Cathepsin B (D1C7Y) XP [®] Rabbit mAb	Cell Signaling Technology	Cat# 31718, RRID:AB_2687580
Mouse TrueBlot [®] ULTRA: Anti-Mouse Ig HRP	Rockland Immunochemical, Inc.	Cat# 18-8817-33, RRID:AB_2610851
p63 (D-9) antibody	Santa Cruz Biotechnology	Cat# sc-25268, RRID:AB_628092
Cathepsin L Monoclonal Antibody (3G10)	Thermo Fisher Scientific	Cat# 415500, RRID:AB_2532191
Cathepsin G Polyclonal Antibody	Thermo Fisher Scientific	Cat# PA5-99402, RRID:AB_2818335
Rat Anti-Mouse C3a Monoclonal Antibody, Unconjugated, Clone 3/11	Hycult Biotech	Cat# HM1072, RRID:AB_533008
Rabbit Anti-Human C3a	Complement Technology, Inc.	Cat# A218
THE [™] DYKDDDDK Tag Antibody [HRP], mAb, Mouse	GenScript	Cat# A01428, RRID:AB_1720817
SGPL1 Rabbit pAB	Abclonal	Cat# A15745, RRID:AB_2763161
Biological samples		

REAGENT or RESOURCE	SOURCE	IDENTIFIER
Malignant melanoma, metastatic malignant melanoma and nevus tissue array, including pathology grade, TNM and clinical stage, 100 cases/100 cores, replacing ME1004g	US Biomax, Inc (Rockville, MD, USA)	ME1004h
Patient-derived xenografts	Laboratory of Ozgur Sahin	N/A
Chemicals, peptides, and recombinant proteins		
4-deoxy Pyridoxine (DPO)	Cayman Chemicals	Cat# 21863
JTE-013	Cayman Chemicals	Cat# 10009458
PF-543	Cayman Chemicals	Cat# 17034
Fingolimod (hydrochloride)	Cayman Chemicals	Cat# 10006292
ABC294640	Cayman Chemicals	Cat# 10587
Corning® Fibronectin, Human, 1 mg	Corning Inc.	Cat# 354008
Cathepsin-L inhibitor (Z-Phe-Tyr(tBu)-diazomethylketone)	Enzo Life Sciences, Inc.,	Cat# ALX-260-134-M001
Geltrex™ LDEV-Free Reduced Growth Factor Basement Membrane Matrix	ThermoFisher Scientific	Cat# A1413202
Sphingosine-1-Phosphate (d18:1)	Avanti Polar lipids	Cat# 860492
D-Luciferin	Selleckchem	Cat# S7763
Ex 26	TOCRIS	Cat# 5833
MK-2206 2HCl	Selleckchem	Cat# S1078
MCC950	Selleckchem	Cat# S8930
CR2-Crry	Laboratory of Stephen Tomlinson	N/A
2ND Gen. Packaging Mix & Lentifectin Combo Pack	Applied Biological Materials (abm)	Cat # LV003-G074
CytoSelect™ 24-Well Wound Healing Assay	Cell Biolabs, Inc	CBA-120
CytoSelect™ 24-Well Cell Invasion Assay (Basement Membrane, Colorimetric Format)	Cell Biolabs, Inc	CBA-110
RPMI-1640	Cytiva	Cat# SH30027.01
DMEM	Cytiva	Cat# SH30243.01
PBS pH 7.4 (1x)	Gibco	Cat# 10010-023
fetal bovine serum	Avantor	Cat # 97068-085
penicillin-streptomycin(100x)	Corning	Cat # 30-002-CI
Plasmocin™ Prophylactic	InvivoGen	Cat# ant-mpp
0.05% trypsin-0.02% EDTA	Corning	Cat# 25-052-CI
Trypan Blue solution	MilliporeSigma	Cat# T8154
MTT Cell Proliferation Assay	ATCC	30-1010K
4% PFA	Boster	Cat# AR1068
10% acetic acid	Fisher Scientific	Cat# 135-32
Pierce RIPA buffer	Thermo Fisher Scientific	Cat# 89900
DTT	Cell Signaling Technology	Cat# 7016L
Protease Inhibitor Cocktail	Sigma-Aldrich	Cat# P8340
PMSF Protease Inhibitor	Thermo Fisher Scientific	Cat# 36978
SuperSignal™ West Pico PLUS Chemiluminescent Substrate	Thermo Fisher Scientific	Cat# 34580
Clarity Max Western ECL Substrate	Bio-Rad	Cat # 1705062
Pierce IP Lysis Buffer	Thermo Fisher Scientific	Cat# 87787
Phosphatase Inhibitor	ThermoFisher Scientific	Cat# 78428

REAGENT or RESOURCE	SOURCE	IDENTIFIER
Magnetic SureBeads protein A or G	Bio-Rad	Cat#1614833
Coomassie	Bio-Rad	Cat #1610786
Duolink <i>in situ</i> hybridization	Sigma-Aldrich	Cat# DUO92101
Puromycin	InvivoGen	Cat#ant-pr-1
Antigen Unmasking Solution, Citrate-Based (pH 6.0)	Vector Laboratories	Cat# H-3300
G418	InvivoGen	Cat#ant-gn-1
QIAzol Lysis Reagent	Qiagen	Cat# 79306
iScript cDNA Synthesis Kit	Bio-Rad	Cat#1708891
SsoAdvanced Universal SYBR Green Supermix	Bio-Rad	Cat# 1725271
BD Cytotfix/Cytoperm Kit	BD Biosciences	Cat # 554714
SuperSignal™ ELISA Femto Substrate	Thermo Fisher Scientific	Cat# 37075
C3a elisa kit: Mouse C3a ELISA Kit	MyBiosource	MBS2506255
RNAscope Hydrogen Peroxide	ACDBio	Cat#322335
RNAscope target retrieval	ACDBio	Cat#322000
RNA scope protease plus	ACDBio	Cat# 322331
RNAscope Detection Kits	ACDBio	Cat# 322360
RNAscope 2.5 HD Duplex Reagent Kit-Hs	ACDBio	Cat#322435
Deposited data		
RNA sequencing data	Gene Expression Omnibus	Accession number: GSE172156
RNA sequencing data	Gene Expression Omnibus	Accession number: GSE169443
Original, uncropped western blot image files	Mendeley dataset	https://doi.org/10.17632/3g49sgnbt.1
Oligonucleotides		
Mm-C3ar1	ACDBio	Cat#476751
Mm-S1pr1	ACDBio	Cat# 426001
Mm-C3	ACDBio	Cat#417841
Mm-IIIb	ACDBio	Cat#316891
Mm-Nlrp3	ACDBio	Cat# 439571
Hs-C3	ACDBio	Cat#430701
Hs-S1PR1	ACDBio	Cat#491201
18S rRNA Forward Primer GTAACCCGTTGAACCCATT	IDT, Coralville	N/A
18S rRNA Reverse Primer CCATCCAATCGGTAGTAGCG	IDT, Coralville	N/A
Mouse S1pr1 Forward Primer ACTACACAACGGGAGCAACAG	IDT, Coralville	N/A
Mouse S1pr1 Reverse Primer GATGGAAAGCAGGAGCAGAG	IDT, Coralville	N/A
Mouse Sgpl1 Forward Primer AACTCTGCCTGCTCAGGTA	IDT, Coralville	N/A
Mouse Sgpl1 Reverse Primer CTCCTGAGGGCTTTCCCTTCT	IDT, Coralville	N/A
Mouse actb Forward Primer	IDT, Coralville	N/A

REAGENT or RESOURCE	SOURCE	IDENTIFIER
GATGCCCTGAGGCTCTTTTCC		
Mouse actb Reverse Primer	IDT, Coralville	N/A
GAGGTCTTTACGGATGTCAACGTCA		
Mouse Nlrp3 Forward Primer	IDT, Coralville	N/A
AGCCAGAGTGAATGACACG		
Mouse Nlrp3 Reverse Primer	IDT, Coralville	N/A
CGTGTAGCGACTGTTGAGGT		
Mouse Il1b Forward Primer	IDT, Coralville	N/A
ATCAACCAACAAGT GATATTCTCCAT		
Mouse Il1b Reverse Primer	IDT, Coralville	N/A
GGGTGTGCCGTCTTCATTAC		
Human NLRP3 Forward Primer	IDT, Coralville	N/A
GGCAACACTCTCGGAGACAAG		
Human NLRP3 Reverse Primer	IDT, Coralville	N/A
GCTCTGGCTGGAGGTCAGAA		
Human IL1B Forward Primer	IDT, Coralville	N/A
CTCGCCAGTGAAATGATGGCT		
Human IL1B Reverse PrimerGTCGGAGATTCGTAGCTGGAT	IDT, Coralville	N/A
Human AIM2 Forward Primer	IDT, Coralville	N/A
CACCAAAAAGTCTCTCCTCATGTT		
Human AIM2 Reverse Primer	IDT, Coralville	N/A
AAACCCTTCTCTGATAGATTCCTG		
Human ACTB Forward Primer	IDT, Coralville	N/A
ACGGCCAGGTCATCACCATTG		
Human ACTB Reverse Primer	IDT, Coralville	N/A
AGTTTCGTGGATGCCACAGGAC		
HumanIL6 Forward Primer	IDT, Coralville	N/A
TGGATTCAATGAGGAGACTTGC		
HumanIL6 Reverse Primer	IDT, Coralville	N/A
TCAGGGGTGGTTATTGCATCT		
Human S1PR1 Forward Primer	IDT, Coralville	N/A
TATCAGCGCGGACAAGGAGAACAG		
Human S1PR1 Reverse Primer	IDT, Coralville	N/A
ATAGGCAGGCCACCCAGGATGAG		
Human CTSL Forward Primer	IDT, Coralville	N/A
ACGCCTTTGGAGACATGACCC		
Human CTSL Reverse Primer	IDT, Coralville	N/A
TGGGGCCTCATAAACAGAG		
Experimental models: Cell lines		
B16-F10 (validated cell line)	ATCC	CRL-6475
4T1 cell line	ATCC	CRL-2539
Myc-CaP	ATCC	CRL-3255
293T	ATCC	CRL-3216
MB49	Laboratory of Besim Ogretmen	N/A
UM-SCC-22A	Laboratory of Besim Ogretmen	N/A
UM-SCC-22B	Laboratory of Besim Ogretmen	N/A

REAGENT or RESOURCE	SOURCE	IDENTIFIER
MDA-MB-231	Laboratory of Philip Howe	N/A
LM2-4175	Laboratory of Philip Howe	N/A
BOM-1833	Laboratory of Philip Howe	N/A
Experimental models: Organisms/strains		
C57BL/6	Jackson Laboratory	Stock# 000664
BALB/c Nude mice	Charles River	inbred/immunodeficient/194
C3aR1 ^{-/-} knockout mice	Laboratory of Carl Atkinson	N/A
Recombinant DNA		
C3 Human shRNA	MilliporeSigma	TRCN0000057139 (Clone ID), 718 (gene ID), NM_000064 (Ref Seq), pLKO.1 vector
C3 mouse shRNA	MilliporeSigma	TRCN0000334476 (Clone ID) 12266 (gene ID), NM_009778 (Ref Seq), pLKO.1 vector
SGPL1 mouse shRNA	MilliporeSigma	TRCN0000173916 (Clone ID) 20397 (gene ID), NM_009163 (Ref Seq), pLKO.1 vector
Ppil1 sgRNA CRISPR/Cas9 All-in-One Lentivector set (Mouse)	Applied Biological Materials (abm)	Cat# 373671140595
CRISPR Scrambled sgRNA All-in-One Lentiviral Vector (with spCas9)	Applied Biological Materials (abm)	Cat# K010
NLRP3 sgRNA CRISPR/Cas9 All-in-One Lentivector set (Human)	Applied Biological Materials (abm)	Cat# 319161110595
Nlrp3 sgRNA CRISPR/Cas9 All-in-One Lentivector set (Mouse)	Applied Biological Materials (abm)	Cat #319161140595
S1PR1 sgRNA CRISPR/Cas9 All-in-One Lentivector set (Human)	Applied Biological Materials (abm)	Cat #429541110595
S1pr1 sgRNA CRISPR/Cas9 All-in-One Lentivector set (Mouse)	Applied Biological Materials (abm)	Cat #429541140595
Plasmid: Mouse S1pr1(NM_007901.5) ORF Clone, pcDNA3.1+/C-(K) DYK	GenScript	Cat# OMu20424D
Plasmid: C3b alpha 2 prime (C3b- α '2) _pcDNA3.1(+)-C-DYK	GenScript	Express Cloning
Software and algorithms		
FlowJo 10.2	TreeStar, OR	https://www.flowjo.com/solutions/flowjo/downloads/
Duolink Image Tool Software	Olink Bioscience	N/A
Prism 8.0.1	GraphPad	https://www.graphpad.com/scientific-software/prism/
CFX Manager 3.1	Biorad	https://bio-rad-cfx-manager.software.informer.com/3.1/
Fiji	NIH Image	http://imagej.net/Fiji
FV10i	Olympus Corp.	FV10-ASW http://www.grapecity.com
GEPIA2	http://gepia2.cancer-pku.cn/#survival	N/A
Akoya Vectra® Polaris™ Automated Quantitative Pathology Imaging system	Akoya Biosciences, Marlborough, MA	N/A
inForm® Software v2.4.10	Akoya Biosciences, Marlborough, MA	N/A
PhenoptrReports Open-Source R Package	Akoya Biosciences, Marlborough, MA	https://akoyabio.github.io/phenoptrReports/index.html